

RAM

● ROBOTICS
AND
MECHATRONICS

AN IMPROVED SOFT-ROBOTIC KNEE BRACE TO ENHANCE THE KNEE STABILITY FOR ACL DEFICIENT PATIENTS

M. (Manasa) Ganesh

MSC ASSIGNMENT

Committee:

dr. ir. J.F. Broenink
dr. ir. H. Naghibi Beidokhti
dr. ir. M. Abayazid
dr. ir. M.A. Marra

November, 2020

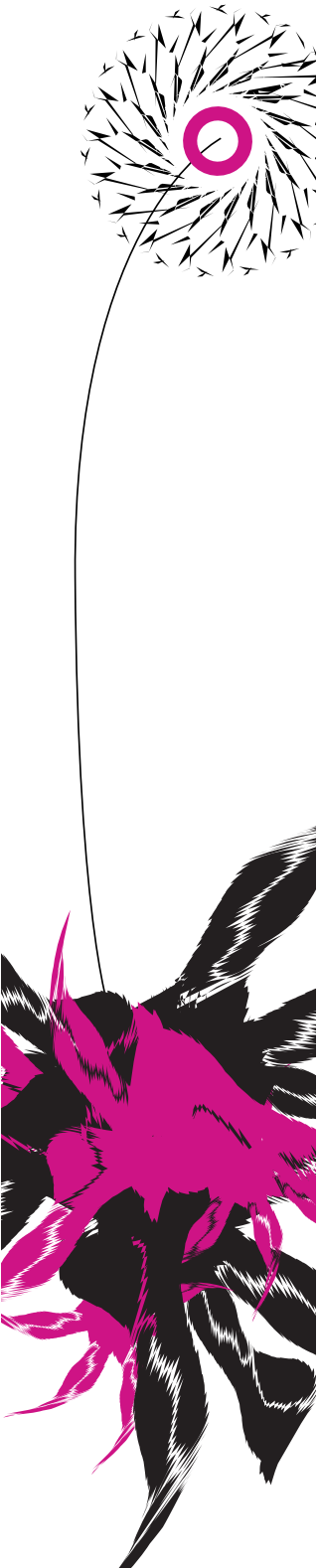
051RaM2020
Robotics and Mechatronics
EEMCS
University of Twente
P.O. Box 217
7500 AE Enschede
The Netherlands

UNIVERSITY
OF TWENTE.

TECHMED
CENTRE

UNIVERSITY
OF TWENTE.

DIGITAL SOCIETY
INSTITUTE



Abstract

Anterior Cruciate Ligament (ACL) is one of the vital ligaments in the knee that stabilizes the joint. It is also the most injured ligament besides the other 3 found in the knee. ACL is injured when the ligament is stretched, partially torn or completely torn, the latter being the commonly occurring ones. Athletes are usually prone to ACL injury risking them to undergo surgical repair, often termed as 'reconstruction', which replaces the ligament from another part of the body. However, surgery becomes an option only in the extreme case. In an initial phase, it is recommended to undergo rehabilitation. One of such techniques to stabilize the joint is by using a knee brace.

Previous study was successful in achieving certain aspects of developing the knee brace. The accomplishments were on studying the dynamics of joint and the role of ACL in controlling the motion of it. It was also successful in making the brace MRI compatible which also enables to study the effect of the brace in limiting the anterior translation of the tibia. The study, however, has been partly successful in achieving the knee dynamics completely. It has only been shown that the brace can achieve a limited range of knee flexion but not the complete achievable range. Apart from linear motion, it lacks the detail on rotational dynamics of the joint in the absence of ACL which is an important consideration.

The focus of this study is to overcome the limitations on the range of flexion by designing for functional range between 0 deg to 90 deg flexion using soft robotic actuation techniques. It is also aimed to study the rotational dynamics of the joint to know if there is a balanced loading of the femur on the underlying cartilage. By designing this, it not only improves the joint stability but also reduces the chances of developing osteoarthritis in a later stage which is very likely to occur for an ACL injured patient. Finally, studying the role of various muscles groups that guides these movements is also into consideration. It is therefore believed that these aspects can enhance the stability of the ACL ruptured joint if implemented.

Contents

1	Introduction	1
1.1	Human Knee	1
1.2	Anterior Cruciate Ligament (ACL)	1
1.3	Deficiency of ACL	2
1.4	Overcoming the deficiency	2
1.5	Problem Statement	2
1.6	Research Question	3
1.7	Design Goals	3
2	Background and Literature review	4
2.1	The Knee: Range of motion and associated activities	4
2.2	ACL rupture: Joint Laxity	4
2.2.1	Anterior Translation of Tibia	4
2.2.2	Internal-External Rotation	6
2.3	ACL Rupture: Muscular Contribution	7
2.3.1	Hamstring Activity	8
2.3.2	Quadriceps Activity	8
2.4	Pneumatic Artificial Muscle (PAM)	9
2.5	Knee Brace	10
2.6	Robotic Knee Brace Approach	10
2.7	Previous Work - Soft Robotic Knee Brace	11
2.7.1	Key aspects	11
2.7.2	Limitations	11
2.7.3	Areas requiring improvement	12
3	Improved brace - Parts design	13
3.1	Design overview	13
3.2	Modified PAM Design	13
3.3	Femur & Tibia support plates and Connecting link	14
3.4	Design of Clamps - Previous work	16
3.5	Downsizing the clamping structures	16
3.5.1	Improving the base ring approach	17
4	Placement layout of PAMs	19
4.1	PAM placement configurations	19
4.1.1	Parallel PAM Configuration	19
4.1.2	Crossed PAM Configuration	20

4.2	Evaluation of placement configurations	21
5	Simulation	23
5.1	Two-link model of the knee brace	23
5.2	Pure translation	24
5.2.1	Model outputs - Pure Translation	25
5.2.2	Choice of damping factor in pure translation	26
5.3	ATT combined with IE	26
5.3.1	Model Outputs - ATT combined with IE	28
5.3.2	Choice of damping factor in ATT combined with IE	30
5.4	ATT Recovery Force - F_{rec}	32
5.5	Division of PAM forces	34
5.5.1	Parallel Configuration	34
5.5.2	Crossed Configuration	36
5.6	Quantification of recovery forces	36
6	Results and Discussion	38
6.1	Recovery Forces - F_{rec}	38
6.2	Quantification of PAM and Recovery forces	39
6.3	Finite Element Simulation - Recovery Force	41
6.3.1	Recovered ATT	42
6.3.2	Recovered IE	43
7	Conclusions	45
7.1	Conclusion	45
7.1.1	Research perspective	45
7.1.2	Design perspective	46
7.2	Further improvements	46
A	Model Import: SolidWorks to Simscape	47
A.1	Initialization	47
A.2	Simscape model - Pure ATT (Figure 5.4)	47
A.2.1	Default blocks	47
A.2.2	Newly added blocks	48
A.3	Simscape model - ATT combined with IE (Figure 5.7)	49
A.3.1	Medial-Lateral representative translations	49
A.3.2	Medial-Lateral representative translations with recovery force	49
	Bibliography	51

List of Abbreviations

ACL Anterior Cruciate Ligament

ATT Anterior Tibial Translation

ACLD Anterior Cruciate Ligament Deficiency

PAM Pneumatic Artificial Muscle

IE Internal-External Rotation

1 Introduction

1.1 Human Knee

Most activities performed on daily basis depends on the motion of the knee. Being the largest joint of human body, knee enables actions such as standing, walking, crouching, jumping and turning. Knee joint comprises of four bones as in Figure 1.1: Femur, Tibia, Fibula and Patella. Femur is round shaped and tibia is flat. Hence besides its functional significance, its structural orientation makes it to be called as the most poorly constructed joint in the body. As a result, a number of other structures also have to coordinate to form a stable knee joint. One of such primary contributors are the ligaments.

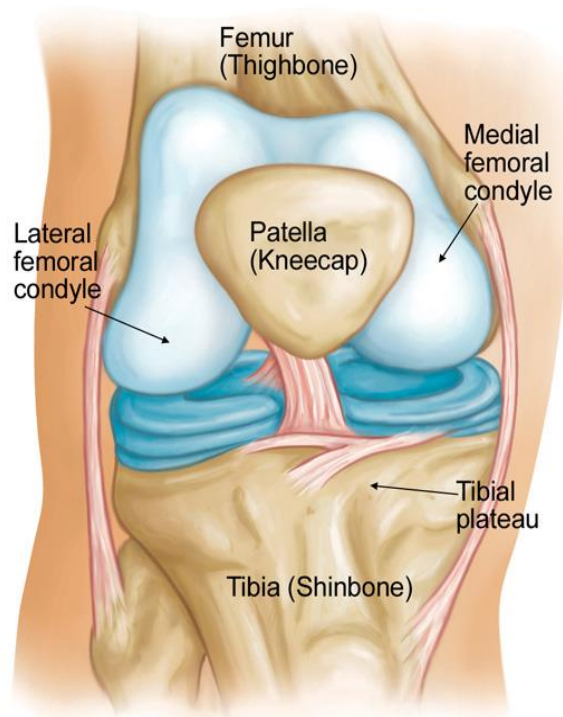


Figure 1.1: Human Knee Anatomy representation from OrthoInfo [2014]

Primarily being connective tissues, ligaments bind between bones. Human knee has four major ligaments namely: Medial and Lateral Collateral Ligaments (MCL and LCL) towards the sides, Anterior and Posterior Cruciate Ligaments (ACL and PCL) crossing each other as X in the knee joint.

1.2 Anterior Cruciate Ligament (ACL)

One of the key ligaments that stabilizes the knee joint is ACL. It is a bundle of collagen fibres which are in parallel. The length of ACL ranges in between 25 to 35 mm in length, 10 mm in breadth and about 4 to 10 mm in width (Marieswaran et al. [2018]). The role of ACL is to restrict the motion of tibia against femur in anterior direction in turn preventing hyperflexion. About 85% of restraining force is provided by ACL to limit the Anterior Tibial Translation (ATT) - Butler et al. [1980], Dargel et al. [2007]. Besides translation, it also helps in controlled tibial Internal and External rotations (IE) around its longitudinal axis by coordinating with PCL.

1.3 Deficiency of ACL

Among the four ligaments, ACL is the most commonly injured one. Injury to the ACL could mean stretching, a partial tear of the fibres or a complete tear, the latter one being the most commonly occurring. The impact of deficiency of ACL depends on the functionality and activities performed by an individual (NHS Foundation [2020]). People participating in sports activity require a lot of movements like changing direction, jumping and pivoting. Besides having an ACL deficient knee, it is possible to cope and carry on with activities. However, this would give rise to the chances of suffering a cartilage damage in a later period if not treated initially.

1.4 Overcoming the deficiency

Depending on the severity of the injury, the treatment would be advised to the patients - Raines et al. [2017]. Athletes, who are most prone to ACL tear, usually choose to undergo surgical reconstruction. This involves replacing the injured ligament by a tendon from hamstring tendon, patellar tendon or quadriceps tendon. Reconstruction does not assure the return of knee functionality back to normal as the neural connections and biomechanics would be lost once the ligament is torn. However, surgery becomes an option only in an extreme case. Patients with low level of activity are initially advised to undergo rehabilitation. Rehabilitation helps in strengthening the knee and its surrounding muscle groups, regain flexibility of knee and also enables normal range of motion. It aims to stabilize the joint once the ACL has been damaged. Yet, opting for rehabilitation is appropriate if the recovery time is not a major constraint (Sports Medicine Institute [2020]). Recovery time may range from a few weeks to months depending on the activity that one might want to return to.

1.5 Problem Statement

With the verge of rehabilitation techniques, several approaches are used to treat Anterior Cruciate Ligament Deficient (ACL D) patients. Use of knee braces to stabilize the joint has been proposed in various biomechanical and clinical researches (Papadonikolakis et al. [2003], Beynnon and Fleming [1998], Xergia et al. [2018] and Kousa et al. [2018]). Though not much is known about the extent of success in overcoming the deficiency of ACL, knee braces are widely prescribed for the avoidance of damage. In the previous study by Khambati [2019], a novel concept of knee brace with pneumatic actuation was proposed which aims to assist recovering the knee stability in ACL ruptured patients.

The research focused on studying the function of muscle groups. It was found that hamstring muscle group increases its activation in order to cope for the deficiency of ACL. The designed soft-robotic knee brace was able to take over the action of hamstrings to a certain extent. Nonetheless, *the brace was designed to perform in a fixed flexion angle of the knee only and the impact of ACL D on IE of tibia was not considered*. Day-to-day activities involves much wider range of motion of knee. To facilitate the usage of knee brace in varying flexion angles, previous design needs to be improved. More number of actuators are required to achieve a dynamic range of flexion. Hence, as a step forward for practical implementation and increasing the range of knee joint functioning, the design must involve actuation at various flexion angles.

1.6 Research Question

By investigating the below questions, it is intended to answer *how to enable multi-directional actuation using pneumatic soft-robotic actuators to maintain the stability of knee during daily activities?* This question is aimed to be answered in the following order:

- Study - What is the prominence of ACL in maintaining an optimal ATT and IE by considering the morphological and neurological factors in ACL deficient knee?
- Analyse - What are the implications of ACL loss on surrounding muscle groups?
- Evaluate - How external forces, internal stiffness and damping factors affect the ATT?
- Design - How to improve the knee brace actuation for a variety of flexion angles suiting the implementation for daily activities?

1.7 Design Goals

The brace must be effective to reduce ATT and ATT combined with Internal-External rotation in ACLD patients. From the previous model of knee brace, the factors which require areas of improvement are considered. Goals derived from the design perspective are:

1. *Components redesign* - For dynamic functioning of the brace, multiple PAMs must be accommodated. This is not possible in existing design as clamping attachments to the PAM are bulky. Thus, the fixing structures need to be more compact.
2. *PAM placement configurations* - The orientation of multiple PAMs must be made appropriately to limit at particular flexion angles. A placement layout needs to be proposed to evaluate how different layouts/configurations impact the functioning of the soft robotic knee brace.
3. *PAM force contribution* - Under different angles of flexion, the range of forces that could be contributed by these PAMs to reduce ATT needs to be quantified.

2 Background and Literature review

2.1 The Knee: Range of motion and associated activities

The two functionalities of knee are extension and flexion. During gait cycle, the angle varies from full extension to a maximum flexion angle depending on the activity. Full extension corresponds to the position when the knee is stretched with the angle between femur and tibia in 0° . Beyond 0° , called as *hyper-extension*, the knee could extend up to a few more degrees only due to the structure of the knee bones. Similarly, flexion corresponds to the angle after 0° and ranging up to 155° . Figure 2.1 from x10therapy [2020] shows an illustration on different activities and the corresponding angles of knee involved. A person must be able to comfortably vary the knee along these angles. However, for regular daily activities such as walking, ascending or descending stairs, chair rising etc, a more limited range up to 90° is required.

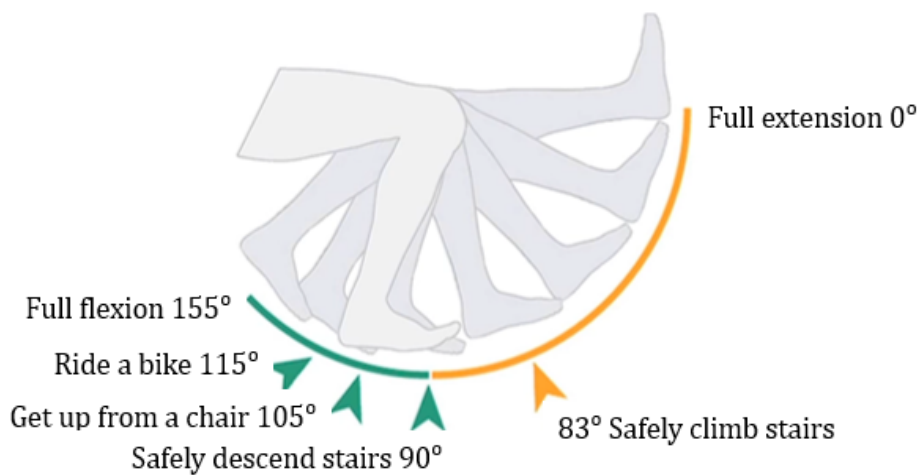


Figure 2.1: Range of motion of the knee and its associated activities

2.2 ACL rupture: Joint Laxity

The tibial and femoral surfaces are not in perfect congruence. Connecting two of the longest bones in human body, the knee joint can move in six degrees of freedom. There are three each translational and rotational movements that can occur as in Figure 2.2. Noyes and Barber-Westin [2017] state that the joint stability is due to the combined effect of active stability from the muscles and passive stability from the ligaments. The hamstrings, quadriceps and gastrocnemius play a dominant role in control of flexion-extension and internal-external rotation of the knee. Besides, this action also gives rise to anterior-posterior shear forces which are controlled by the cruciate ligaments. It is therefore crucial to understand that the term instability could be understood as giving way by knee joint due to one of the above factors and hence cannot be generalized.

The scope of this research is to focus on the instability occurring due to inappropriate ATT and IE condition since the increased laxities are observed more to be in ATT and IE after ACL rupture.

2.2.1 Anterior Translation of Tibia

As referred from papers Dargel et al. [2007] & Rachmat et al. [2016], ACL produces maximum restraint of more than 80% against anterior translation of tibia. The magnitude of translation

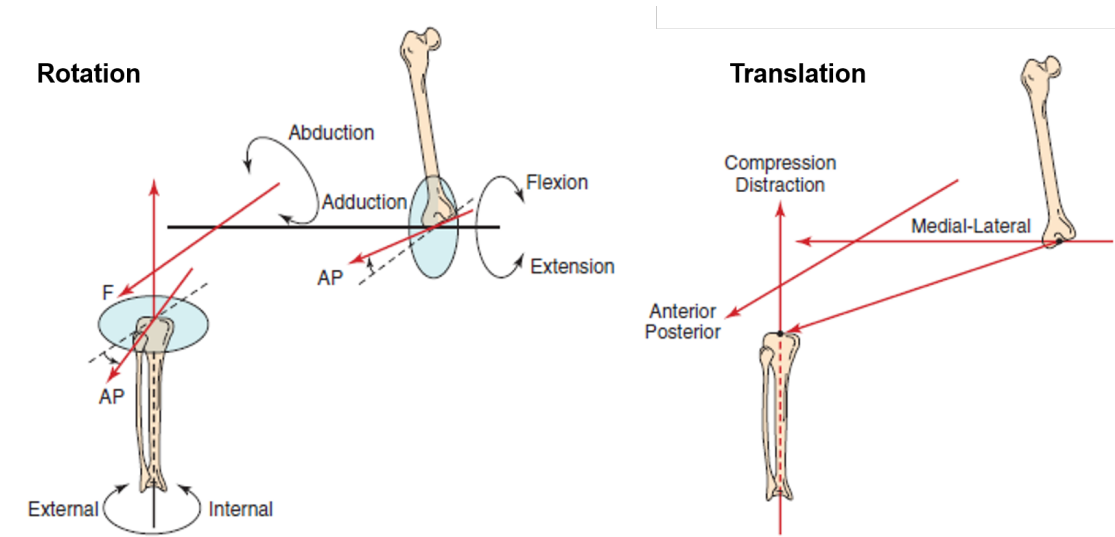


Figure 2.2: Rotations & Translations of knee joint as illustrated by Noyes and Barber-Westin [2017]

increases proportional with applied loading forces. With the simulation of the femur-joint it is possible to assess the translation under different loading conditions. Same has been proposed in Papadonikolakis et al. [2003]. From Butler et al. [1980], it was shown that for 90 degrees of flexion, ACL provided an average of $85.1 \pm 1.9\%$ of the total restraining force as in Figure 2.3. A

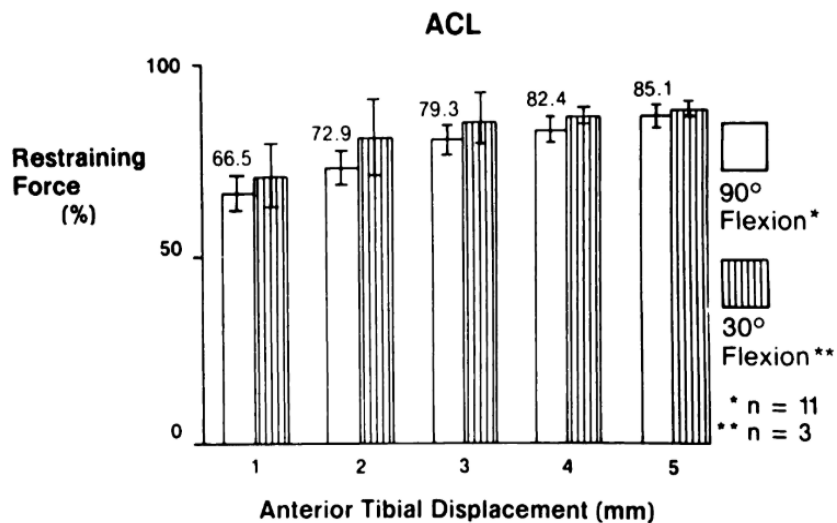


Figure 2.3: Anterior drawer results without rotation obtained by Butler et al. [1980]

similar average $87.2 \pm 1.6\%$ was found at 30 degrees. The average restraining force in the intact knee was about 440N at 90° and approximately 333N at 30°.

In case of ruptured ACL, hamstrings play a major role in restoring the tibial displacement. The results from Papadonikolakis et al. [2003] showed that by simulated hamstring force at 56% of its maximal isometric strength, near normal anterior-posterior translation in the ACLD knee was restored. Shelburne et al. [2005] proved that it was possible to reduce ATT in the ACLD knee to the level calculated to the level of intact knee with increased magnitude of hamstrings force. Besides, the research by Beynnon and Fleming [1998] found that that under unloaded conditions, bracing not only reduced ACL strain values for anterior directed loads applied to the tibia but also reduced strain values in response to internal-external torque applied about

the long axis of the tibia. These results provide a strong evidence that with externally providing these restoring forces by supporting hamstring activation via the proposed model of brace, it might be possible to restore the anterior tibial translation as to the extent of intact knee.

2.2.2 Internal-External Rotation

The surfaces of femoral medial and lateral condyles are distinct as mentioned in Section 2.2. The lateral surface has a higher variation than medial as in Figure 2.4. The medial meniscus has a deeper femoral surface and is more firmly anchored than the lateral meniscus. The lateral meniscus has more mobility from its restraining ligaments. The displacement of lateral meniscus is as much as two times further posteriorly than the medial meniscus during knee flexion. This suggests that the longitudinal axis of rotation is medially located - Smith et al. [2003].

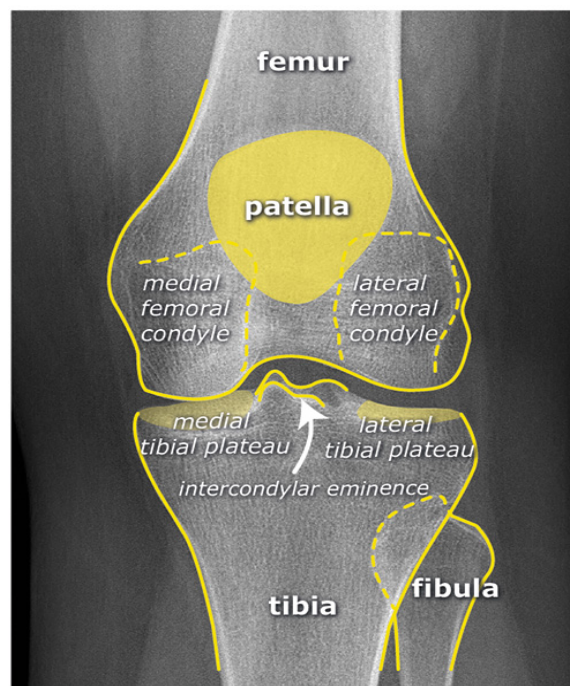


Figure 2.4: Medial and lateral femoral condyles

Several approaches are discussed in Jones and Grimshaw [2011] to analyse the axis of tibial rotation during flexion and extension. In one of the approaches by Brantigan and Voshell [1941], the axis is closest to the joint surface during flexion, allowing ACL and other ligaments of the joint to slacken. In extension, the axis is further away from the joint line and the same ligaments become tense. This axis is referred as *instantaneous axis*. However, the drawback with this approach was that the condyles of femur are varied in three dimensions rather than two dimensions while the axis of rotation can only be in two dimensions.

To study the effect of ACL loss on internal and external rotation, it is important to first analyse the rotation in the presence and absence of ACL. By bisecting the ACL and finding the difference in rotation range before and after dissection, Lipke et al. [1981] concluded that ACL indeed caused significant changes in the range of rotation. With this, it was also concluded that with the loss of ACL, the rotation axis shifted towards medial side. Noyes and Barber-Westin [2017] points that if the motion is limited to translation, the point does not depend on whether the axis is towards medial or lateral side as the path is parallel. But when combined with rotation, translation no longer depends on the same point - Figure 2.5.

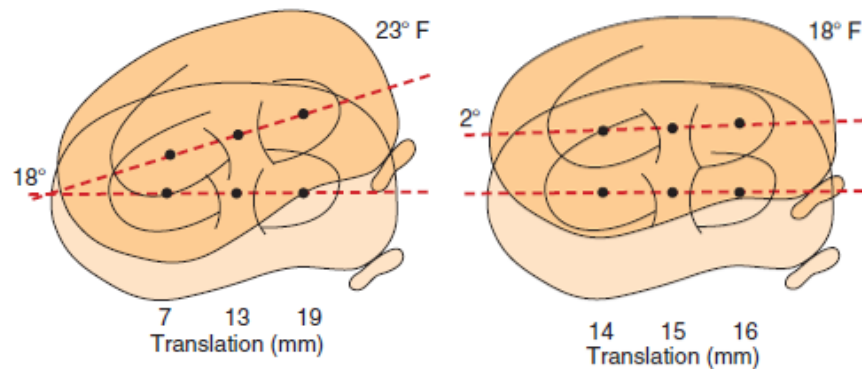


Figure 2.5: Left - Translation with higher IE rotation with greater unequal displacement, Right - Translation with less IE rotation and lesser unequal displacement (Noyes and Barber-Westin [2017])

Hence, it becomes important to decide the axis of rotation as each of the above mentioned approaches lead to different results varying between center of tibial longitudinal axis towards the medial side with the increasing flexion angle - Feng et al. [2015]. Because the condition varies from every patient, the center of rotation is assumed based on closest axis to the center of tibial longitudinal axis as an initial approach in this research. Therefore, the point lies in the center of tibia based on which medial and lateral translations are calculated.

2.3 ACL Rupture: Muscular Contribution

Hamstring and Quadriceps are the two major muscle groups involved in achieving the flexion and extension angles. By forming agonist-antagonist pair, the two co-ordinate to vary the angles of knee - Figure 2.6 (Wilson [2019]). During extension, quadriceps act as agonist mus-

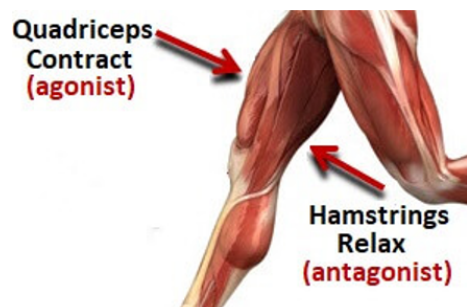


Figure 2.6: Association of hamstrings and quadriceps with knee joint.

cle generating high forces to contract. While hamstrings being antagonist, provide low level of muscle activation termed as co-contraction - Hirokawa et al. [1991]. Similarly, the function is reversed during flexion. The balanced coordination between the two muscle groups is one of the main reasons behind controlled knee movements.

A number of factors contribute in maintaining the stability of the knee joint. As per Lam et al. [2002], the functional instability is caused by anterior translation of tibia as well as impacted co-ordination of the muscles. ACL, primarily being a bundle of collagen fibres, contains mechanoreceptors. These receptors in coordination with the other ligaments of the knee, transmit the sensation relating to joint movement and joint position to the brain by proprioception as stated in Johansson et al. [1991], Dhillon et al. [2011]. When ACL is ruptured, sensory feedback by these receptors is also diminished causing affected muscle coordination. It was also observed that with remnant ACL fibres, the functional recovery is still a possibil-

ity if these receptive fibres again grow into the reconstructed ligament (Dhillon et al. [2011]). However, in the method of grafting, the injured ligament is often removed totally to insert the new graft. This also suggests that retaining of these receptors in this case is not possible. From the above explanation, one could infer that reconstruction in many instances may not be the choice to go for.

Rehabilitation, on the other hand, follows the approach of balancing muscle activation levels. With the loss of ACL, the adaptation of muscle groups to perform various daily activities become altered to overcome the deficiency. As stated in Paterno [2017], by assisting the muscles activation levels, it is possible to gradually regain the functional stability of the joint. To analyse the activation of these muscles in ACLD, it important to first understand the individual changes in behavioural pattern that Quadriceps and Hamstrings undergo when ACL is ruptured.

2.3.1 Hamstring Activity

Several studies suggest that hamstring activation level differs in ACL deficient knee when compared to a normal knee and also with the level of activation of quadriceps - Aalbersberg et al. [2009], Liu and Maitland [2000]. Knowing that loss of ACL leads to increased anterior translation of tibia, with increased hamstring muscle activation levels upto 56% of its maximum, the tibial translation could be returned to its normal level. This was found possible in combination with joint contact and quadriceps forces as mentioned in Shelburne et al. [2005]. Activation of hamstrings during loaded flexion reversed the posterior force acting on tibia as discussed in MacWilliams et al. [1999]. The results also suggested that besides reducing loads at ACL, hamstrings required more energy to maintain flexion and increased loads at patellofemoral and tibiofemoral joints. This increased activation could be considered as a protective mechanism as described by Begalle et al. [2012] and Bryant et al. [2008]. Proper training of hamstring muscles by rehabilitation enhances the possibility of returning to sport activities.

In the research by Khambati [2019] performed in the department of Robotics and Mechatronics at University of Twente, externally activated PAM muscles in the knee brace coordinated with the hamstring activation. By externally supporting the activation of hamstring muscles, it shared a part of the overall load acting on hamstring muscles.

2.3.2 Quadriceps Activity

Quadriceps is known to be weakened after the loss of ACL (Lynch et al. [2012]). Weakening here refers to its inability to activate fully due to the structural changes in the joint. As mentioned in Section 2.1, the loss of mechano-receptors leaves the condition irreversible. Quadriceps activation failure can thereby lead to quadriceps strength deficits and may also act as a constraint for rehabilitation. Analysing the reasons for quadriceps weakness becomes an important aspect to further decide the treatment of ACLR patient. According to Buckthorpe et al. [2019], the strength of the muscle not only depends on neurological factor but also on morphology therefore making them interdependent. Williams et al. [2005] reported that quadriceps weakness is a combined result of quadriceps activation failure and quadriceps atrophy.

The way of measurement of quadriceps weakness is another key aspect in determining the extent of strength that needs to be restored in the muscle. As per Petterson et al. [2008], the extent of weakness in ACLR knee is often compared against the contralateral limb. The research also points that though ACL injury is unilateral, the occurring weakness post injury is bilateral lasting upto two years post reconstruction of ACL. Therefore, using the contralateral limb's strength as a mark of measure is suggested to be far from ideal condition. It is also noteworthy that the suggested stable reference to measure could rather be non-reconstructed legs as its strength was found to be in between that of reconstructed and control legs. This could also act as an advantage in our study to indicate the performance of rehabilitated legs over reconstructed ones given that factors considered in both cases are similar with not much of dissimilarities.

2.4 Pneumatic Artificial Muscle (PAM)

PAMs are contractile or extensional devices operated by pressurized air filling a pneumatic bladder. Early PAMs were made use as artificial limbs named as McKibben muscles. The purpose of using these muscles is that they are lightweight, easy to fabricate, have a maximum contraction and have load-length curves similar to human muscle - Roche [2020]. At maximum activation, they contract ranging from 25% to 40% of their original length depending on the material involved. This ability to contract makes PAMs to be used as artificial muscles. In the research by Khambati [2019], the hamstring muscle activation was supported by means of externally actuated pneumatic artificial muscles. Contraction ratio (ϵ) of PAM can be calculated based on Equation 2.1, where l_0 and l are the initial and shortened length of the PAM respectively.

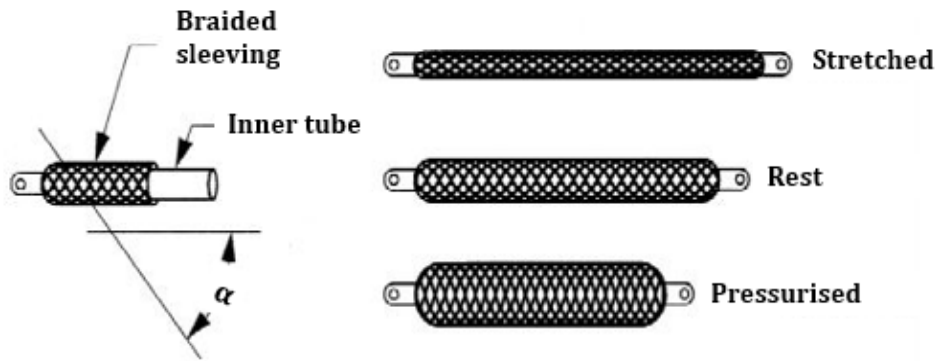


Figure 2.7: McKibben muscle from Daerden and Lefeber [2002]

The force produced by PAM depends on its design with the deciding factors being *length* (l), *diameter* (D) and *braid angle* (θ). The overall length of the muscle does not contribute to the force, but only as supporting structure. The active length is the length of the bladder within the muscle which expands in volume when pressurized. The diameter of the bladder determines the force that it can produce. Higher the air pressure, higher the force that can be produced. However, the thickness of the bladder should also be chosen wisely to obtain the appropriate force. If the bladder thickness is slim, it cannot withstand high pressure and expands out of the braid. If too thick, the contraction force of the muscle reduces as its ability to hold larger pressure reduces. The braid sleeve around the PAM limits the maximum contraction length depending on the braid angle.

The relation between ideal force exerted, length and diameter of PAM is represented in Daerden and Lefeber [2002] by the equations below:

$$\epsilon = \frac{l_0 - l}{l_0} \quad (2.1)$$

$$F_{ideal} = \frac{\pi D_0^2}{4} P [a(1 - \epsilon^2) - b] \quad (2.2)$$

where F_{ideal} is the ideal force exerted by the PAM, D_0 is the initial diameter of PAM when in rest state and P is the supplied pressure. Considering α_0 and α as initial and contracted length braid angles respectively, a and b can be estimated as:

$$a = \frac{3}{\tan^2 \alpha_0}$$

$$b = \frac{1}{\sin^2 \alpha_0}$$

2.5 Knee Brace

Knee braces are designed with the goal to stabilize the underlying conditions of the knee illustrated as in Figure 2.8. As discussed in Section 1.4, the treatment of knee injury is wholly dependent on the severity of injury. Referring to Miller [2020], based on the functional requirements, knee braces are categorized to several types.

1. **Prophylactic** braces protect the knees from injuries during contact sports
2. **Functional** braces support already injured knees
3. **Rehabilitative** braces limit harmful knee movement after an injury
4. **Unloader/off-loader** braces provide relief to arthritis patients with knee pain



Figure 2.8: A commercially available rehabilitative knee brace from Doc Ortho [2020]

In the studies by Beynnon and Fleming [1998], Xergia et al. [2018] and Kousa et al. [2018], the effectiveness of using functional knee braces to stabilize the ACL deficient knees have been investigated. Beynnon et al. [1992] studies the performance of off-the-shelf and custom-made braces available to examine the stability deciding factors such as Anterior-Posterior Shear Loading, Internal and External Torques of the Tibia and Active Range of Flexion-Extension of the Knee. The results determined that these braces could help stabilizing the joint in a relatively lower anterior loads (less than 100 N). However, in daily activities, the loads are perhaps of higher magnitude. As per Noyes and Barber-Westin [2017], it was reported that the loads in daily activities ranges between 0 N to 454 N.

Commercial braces which are universal might cause general non-effective constrain to the knee irrespective of the severity of ACL rupture. Moreover, their fully passive structure limits the range of motion even when their constraint is not needed. Therefore, the study recommends further investigation to categorize the design to individually assess different factors that define the stability of knee. These aspects, if implemented, may possibly improve the effectiveness of the brace.

2.6 Robotic Knee Brace Approach

The effectiveness of hamstrings and quadriceps muscle groups are adversely affected on account of an ACL tear. As discussed in Section 2.3.1, hamstrings play a significant role in re-

stricting unwanted anterior translation of tibia in the presence and absence of ACL. However, in the absence of ACL, the effectiveness of hamstrings is observed to be reduced. The research by Xergia et al. [2018] emphasizes the need to develop pre-programmed compensatory muscle activation strategies. By implementing feed-forward strategies, it is expected to initiate hamstring co-contraction and improve chances towards a stable knee via hamstring conditioning.

2.7 Previous Work - Soft Robotic Knee Brace

In the previous research by Khambati [2019], a soft robotic knee brace was implemented. The brace functioned with the help of a pair of PAMs on either side of the knee. By pressurizing these, it was able to take-over the load of hamstrings up to an extent. The aspects of this design and its limitations discussed below provide insight on areas of improvement which becomes the focus of this research.

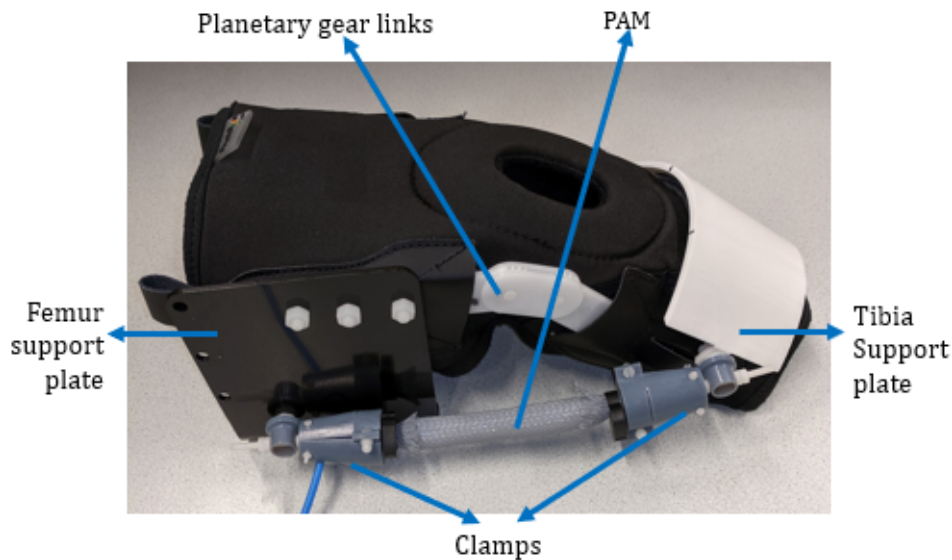


Figure 2.9: Soft robotic knee brace developed by Khambati [2019]

2.7.1 Key aspects

A short summary of the model of robotic knee brace developed by Khambati [2019] is listed below. A few aspects have been retained from this model to maintain the working concept of the previous brace while much have been improvised to facilitate the improved functioning. The detailed update on design modifications are discussed under Chapter 3.

- The components were support plates for tibia and femur, Pneumatic Artificial Muscles (PAMs) and planetary gear links integrated into a commercially available knee brace - Figure 2.9.
- PAMs were clamped on to the support plates with custom designed clamps. Attached along the sides such that when activated, PAM forces reduce the level of hamstring activation.
- The brace aimed at reducing the anterior translation of tibia by assisting hamstrings at a certain angle of flexion.
- Summarizing, increased level of hamstring activation was partly taken over by the brace.

2.7.2 Limitations

The functioning of this brace had its constraints. Such as:

1. **Functioning range:** The discussion in Chapter 2 points that the functioning range of human knee ranges from 0° to 90° on the basis of daily activities. The existing prototype is not designed to function beyond 30° flexion.
2. **Number of PAMs:** By activating a single set of PAMs, the range of flexion cannot go beyond 30° since the PAMs have a limited functional length. Therefore, during flexion, only one actuated PAM can not cover the whole range of flexion i.e. 0° , 30° , 60° and 90° . PAM becomes out of use if shortened beyond a limit.
3. **Space crunch:** Accommodating more PAMs in the existing design cannot be made due to limited space available. This creates a necessity to minimize/modify the design of existing components.
4. **IE Rotation:** Even though the brace proved to support hamstring activation, the study did not focus on analysis of Internal-External rotation which is simultaneous with ATT in an ACLD knee.

2.7.3 Areas requiring improvement

Considering the above mentioned limitations, areas requiring improvement from the previous design can be proposed. The areas of improvement focus on enhancing the functionality of the brace by reviewing the following factors:

1. Implement brace design to prevent the anterior translation of tibia for flexion multiple angles of knee. Namely, at 0° , 30° , 60° and 90° of flexion.
2. This would need 4 sets of PAMs placed along either side of the knee. With changing angles of flexion, activation of PAMs must be controlled.
3. With modified design of clamp, analyse the clamping forces to withstand the forces of PAM.
4. Modify the existing support structures of femur and tibia in order to accommodate a total of 8 PAMs - 4 on each side.
5. Design the layout for proper placement and fixing of these muscles in order to achieve defined flexion ranges.

3 Improved brace - Parts design

3.1 Design overview

This chapter focuses on the improvement or modification of soft-robotic knee brace parts design from Khambati [2019] to make them feasible in the improved soft-robotic knee brace design. The basic parts combined into the assembly are shown in Figure 3.1. The figure shows an illustration of PAM in the clamping holes. Chapter 4 explains in detail the placement configurations of PAM in these clamping holes. This section focuses on the design details of PAM, femur and tibia support plates, connecting links and finally the clamps. With the proposed new design, it is intended to overcome the limitations of design as mentioned under Section 2.7.2.

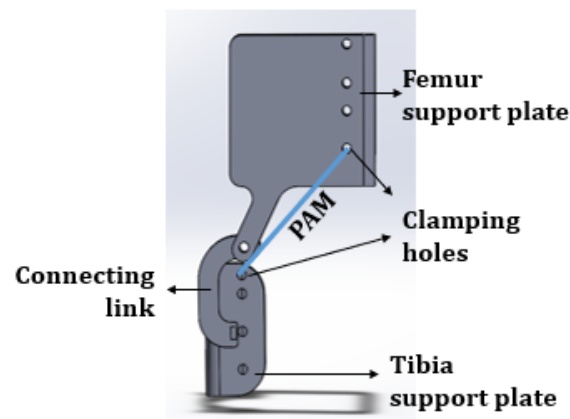


Figure 3.1: Proposed 3D model of the soft robotic knee brace

3.2 Modified PAM Design

Considering the fact that the PAMs produced satisfactory forces in fixed angle of flexion in the research by Khambati [2019], it is convenient if the approach is adapted to be used for multiple angles of flexion with multiple PAMs making the design dynamic. However, the total length of the original PAM is increased to 200 mm to accommodate the support ends (Figure 3.2).

Table 3.1 shows the comparison between modified and original size of PAM. The slim ends of the PAM are designed to act as supporting structures during clamping. The dimensions of bladder are retained from the previous design to obtain same value of force v/s pressure characterization curve. The overall length of PAM shown in Figure 3.2 is modified to meet the hole distances between tibia and femur plates while the overall diameter of the PAM itself is retained inclusive of the diameter and length of the bladder. The length of the bladder was retained to be 90 mm from the previous research.

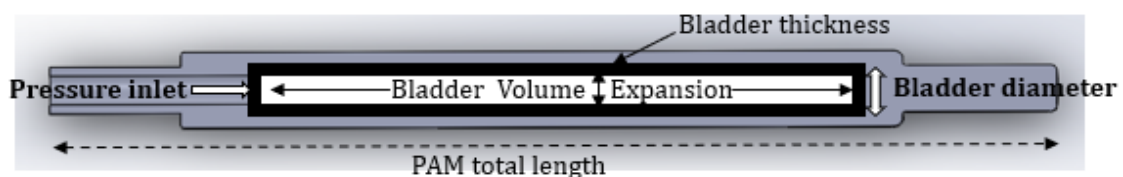


Figure 3.2: Cross section of PAM model

Choice of maximum contraction length: Section 2.4 mentions the length of PAM after activation is 12% of its original length (Khambati [2019]). This contracted length can only be used

Dimensions	Total Length mm	Length of Bladder mm	Outer Diameter mm
Original	120	90	14
Modified	200	90	14

Table 3.1: Comparison of PAM dimensions

when the design is fixed to a certain flexion angle. When subjected to flexion angles such as 30°, 60° and 90°, the distance between the clamping holes on femur and tibia plate for each PAM reduces.

When the distance between the clamping holes is lesser than the PAM's maximum contraction length, then the PAM can no longer produce the required force of 50N. Considering the case of modified PAM with added support ends, the modified length is higher than the original length. This necessitates the need to increase the maximum contraction length threshold from 12%. As an initial step, the threshold is increased to 25% providing additional room for added support ends. Thus, the maximum contraction length is considered to be not more than 25% of its original length.

In the context of multiple PAM based actuation, it becomes a subject of research if the length of PAM has to remain constant in all the actuators in the design or if it has to be varied. This will be further discussed under the Section 4.1

3.3 Femur & Tibia support plates and Connecting link

The femur and tibia plates act as supporting structures to femur and tibia respectively. The positioning of these support plates has to be made such that required force from the PAMs is transferred at every angle of flexion. Figure 3.3 and Figure 3.5 shows the 3D models of tibia and femur plates. Both these structures have a common point to connect the connecting link. Each of these plates have sets of four holes on each side to fix the clamps that hold the PAMs. Tibia support plate has a slider hole that allows for the translation of connecting link - Figure 3.4 (a). The stages of translation occurring in the prismatic slider is illustrated in Figure 3.4 (b) & (c).

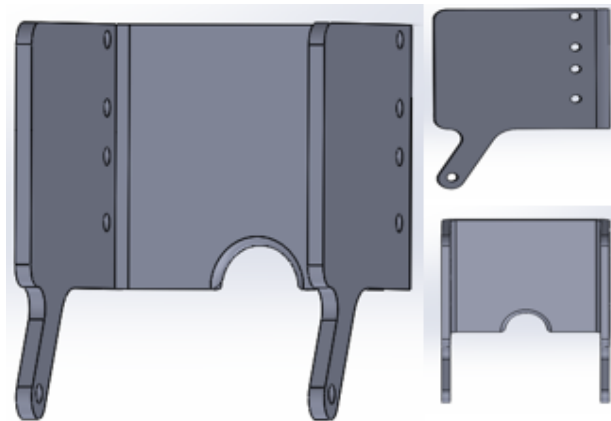


Figure 3.3: 3D design of Femur support plate

The support structure of tibia has a curved inner surface while the outer surface is near flat to accommodate the slider as well as PAM clamping holes. The choice of position of these holes is based on the required PAM forces in every angle of flexion. With the vertical positioning of holes, it is expected to achieve higher magnitude of PAM force in the direction opposite to ATT than horizontally positioned holes. The detailed analysis of placement layout of PAMs is discussed under Section 4.1.

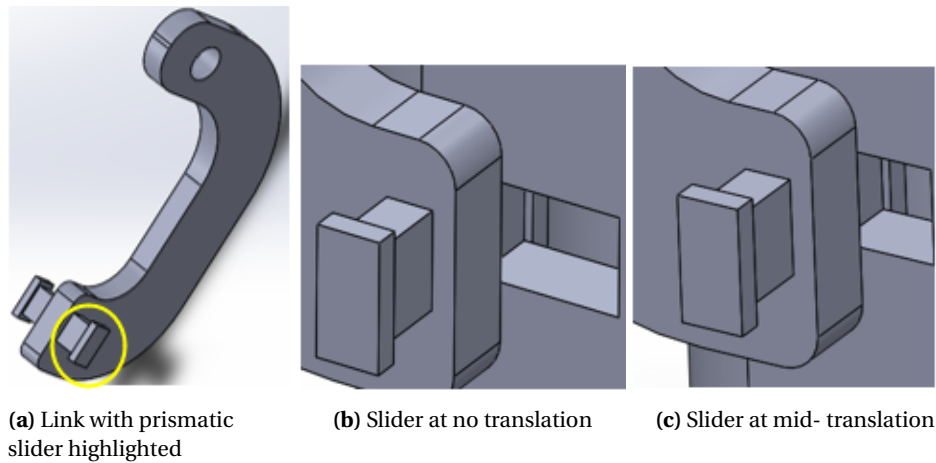


Figure 3.4: Link with concentric hole connecting to femur plate and prismatic slider connecting tibia plate

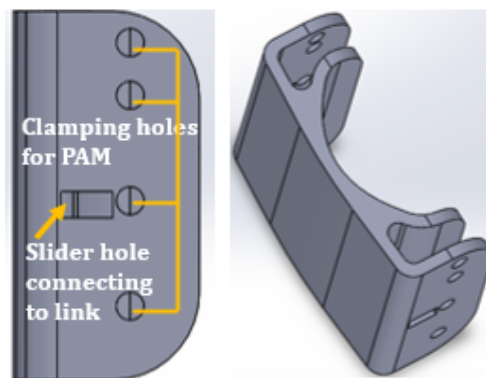


Figure 3.5: 3D design of Tibia support plate with holes for slider and PAM clamps

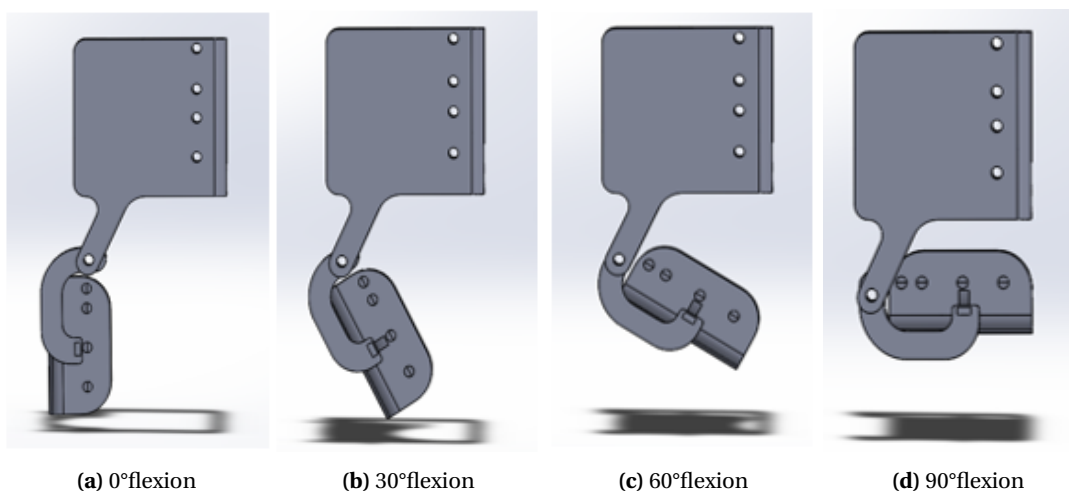


Figure 3.6: Flexion angles illustrated in improved design of brace

The assembled model of brace with femur and tibia plates at flexion angles 0°, 30°, 60° and 90° is shown in Figure 3.6.

3.4 Design of Clamps - Previous work

Clamps are support structures that connect PAMs to tibia and femur support plates. The clamps must be able to withstand the axially directed force that is exerted by the PAM. As observed under the research by Khambati [2019], the force of friction between the braid and the clamp is much lower than axial force of the muscle causing the clamp to slip away from the braid. To overcome this, another supporting ring structure to the clamps were designed that helped the clamps withstand the axial force. Figure 3.7 shows the clamp design with support rings in previous research inspired from the concept by Mori et al. [2010].

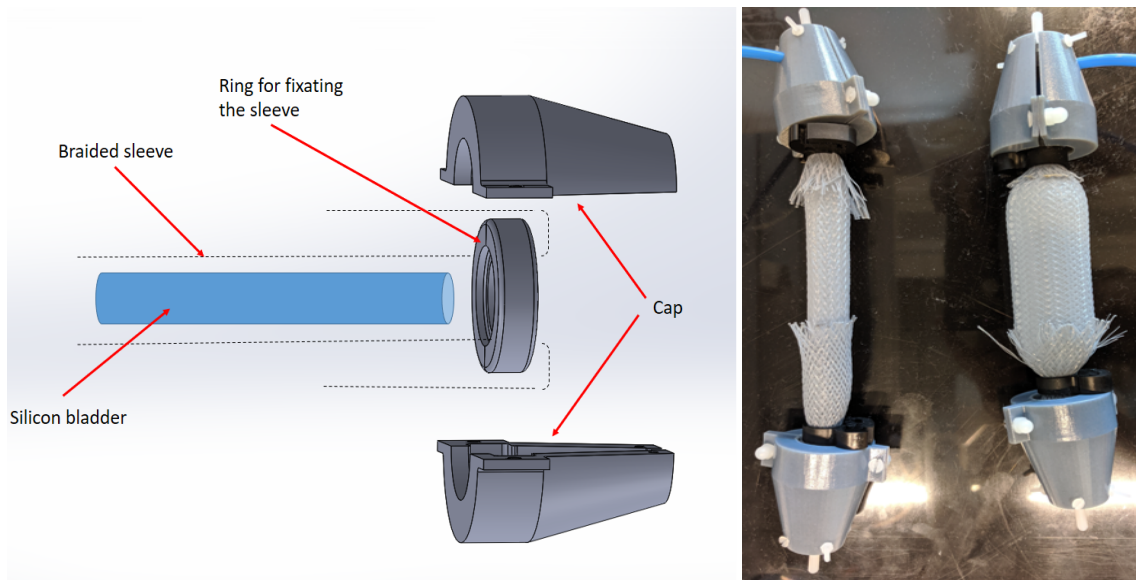


Figure 3.7: Design of clamping structures by Khambati [2019]

As illustrated in the Figure 3.7 (left), the braid enclosing PAM is wrapped around the base ring and cased using end caps. The cap is then connected to the femoral and tibial support plates. The figure to the right shows the clamps assembled to the PAM under relaxed and pressurized conditions. From a functional perspective, the design can withstand the PAM forces. Meanwhile, from the design perspective, the inclusion of such wide base rings makes it a bulky fixture. As the purpose of the design was intended to function in a single angle of flexion, the bulky clamps did not pose a limitation.

3.5 Downsizing the clamping structures

The improved model of brace requires downsizing of these clamps with a modified design. The dimensions of each of the caps are 40mm^2 . Considering the placement layout of the PAMs mentioned under Section 4.1, the dimension of femur support plate is $120\text{mm} \times 110\text{mm}$. With this data, it is evident that the support plates can only accommodate a maximum of two such clamps which is not feasible in the improved design.

Clamping requirements in the improved design:

- Since the number of PAMs on either side of the support plates is 4, the size clamps should be compact enough to attach 4 of these in every side of the support plates.
- The placement of these clamps should not be fixed in a single point but allow rotation along the point of fixation. Since PAMs are flexible structures, at every changing angles of flexion, the slackness in the middle of PAMs causes rotation along its fixing points.

3.5.1 Improving the base ring approach

The base ring concept indeed supports the overall load bearing capacity. Nonetheless, as seen in Figure 3.7, the base ring encircles around the PAM adding more to the existing diameter of the PAM. Therefore, the idea was to reduce the diameter of the non-inflating diameter of PAMs. The term *non-inflating* refers to the support ends of the PAM which are designed to only act as supporting structures. By covering this area with support rings reduces the extent of radial increase of the PAM volume. Figure 3.8 below demonstrates the modified PAM diameter for base ring attachment around the end support structures.

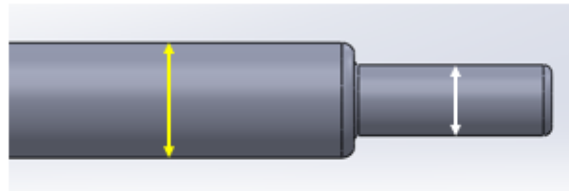


Figure 3.8: Outer diameter indicated by yellow arrow and reduced diameter by white to accommodate base ring

The modified design of base ring is proposed as a bi-layered cylinder (inner and outer layers). By categorizing the layers, it is intended to take the best advantage of the friction force between the materials. The inner layer, indicated (2) in Figure 3.9 (a), that is in contact with the braid is 3D printed in Agilus material which is a durable, rubber-like photopolymer simulating the look, feel and function of rubber (Source: Stratasys [2018]). The outer layer, indicated (1) in Figure 3.9 (a), is a harder material made of VeroWhite that helps transfer of force to the clamps. The outer surface of the outer layer is patterned with sharp teeth-like structures to create friction between holes in expanded braid and the teeth patterns. When braid expands, the holes in the braid are intended to house in between these patterns. The cylinder is designed with an open edge such that when the ring is compressed, it wraps around the diameter of the PAM support ends Figure 3.9 (a) & (b).

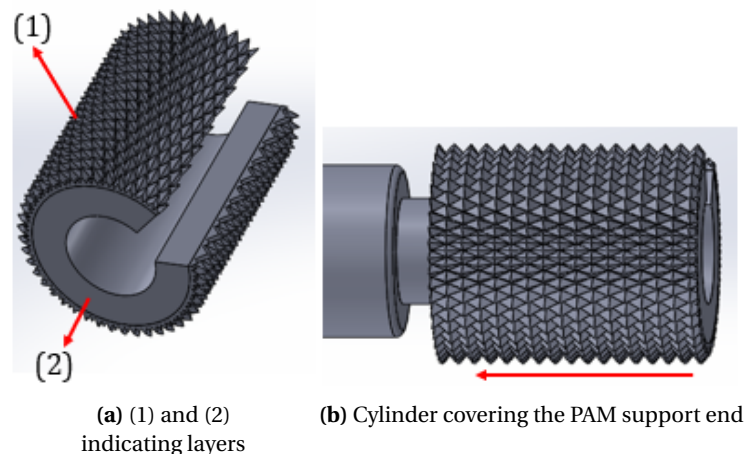


Figure 3.9: Bi-layered cylinder covering the PAM support ends.

The PAMs covered with the bi-layered cylinder has to be mounted to the support plates of tibia and femur. Hence, a clamping structure that links between PAM-cylinder and support plates is designed. As mentioned in Section 3.5, the clamps have to hold the PAM and rotate along its point of fixation.

Figure 3.10 shows the design of clamp. The rear end is bolted with 8.5mm thread to the femur and tibia support plates with enough force to allow the rotation of clamping structure. This

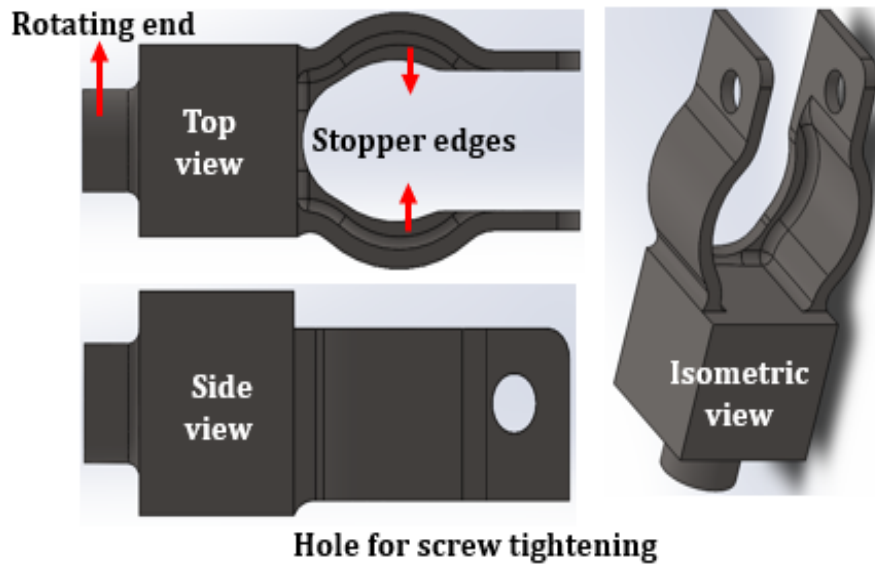


Figure 3.10: Proposed design of clamp to house bi-layered cylinder and PAM

gives room to the PAMs to orient in different angles during changing angles of flexion. The front-end is has wide opening that closes when threaded through the hole. This ensures holding the cylinder firm within the clamps. Besides compressing with bolt, the stopper designed in the bottom of the clamp prevents the possibility of the bi-layered cylinder sliding downwards when PAM undergoes compression and a pulling force exerts on it. Figure 3.11 illustrates the PAMs clamped to the femur supporting plate.

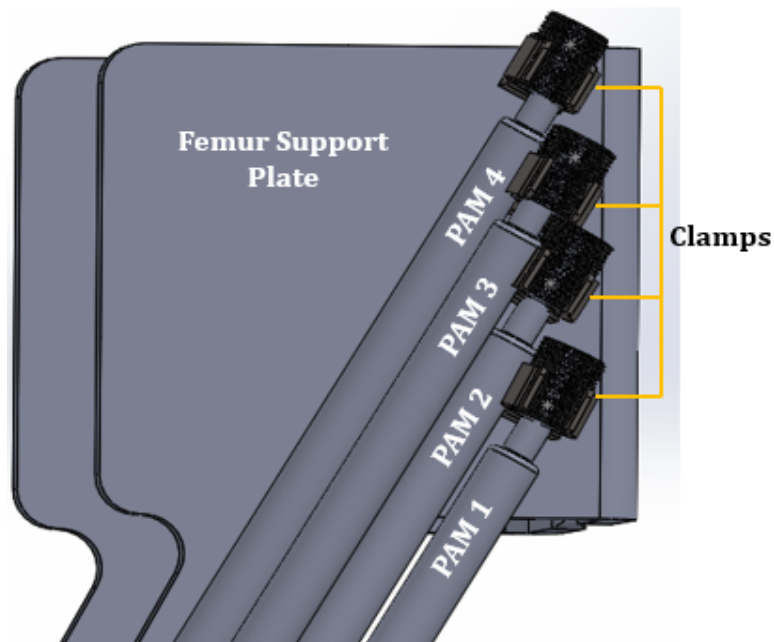


Figure 3.11: PAMs assembled to the clamps in femur support plate

4 Placement layout of PAMs

4.1 PAM placement configurations

The placement of PAMs on the brace must be made such that the PAMs are functional in all flexion angles of the knee. This ensures the usability of PAM in different gait cycle activities. Though various configurations are possible to place the PAM to the clamping hole, it is necessary to determine the effectiveness of the PAM once the knee undergoes flexion. In this research, two configurations for the placement of PAMs are proposed and its extent of usability is analysed. Figure 4.2 illustrates the parallel and crossed PAM configurations of the brace.

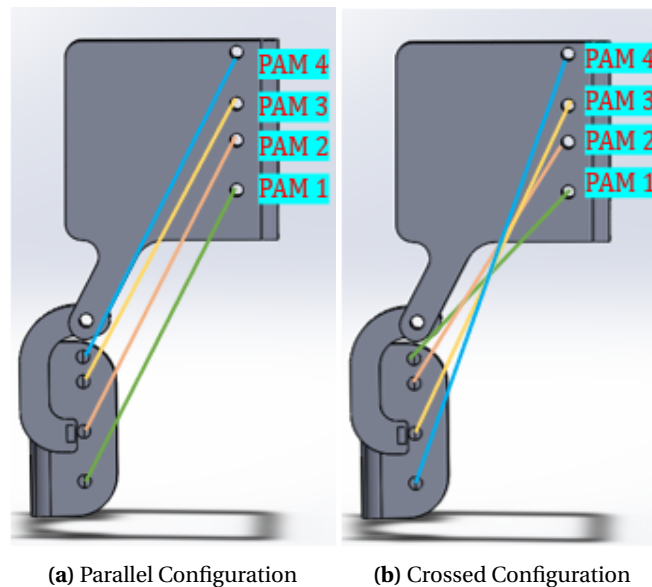


Figure 4.1: Proposed parallel and crossed PAM configurations of the brace.

Both these configurations are evaluated using two factors that further help quantifying the contribution of individual PAMs. The factors considered are:

1. **Preserved length of PAM at every flexion angle:** The total length of PAM reduces as the knee flexes to increasing angles. This reduced length of PAM is known as *Preserved Length*. As mentioned in Section 3.2, if the length of PAM before actuation is less than its maximum contraction length, then the contribution of the PAM is considered to be null.
2. **PAM Angle:** The angle made by the PAM along the x -axis is required at every angle of flexion as the force of PAM is measured along the cosine component. Therefore, a lower value of θ yields higher magnitude of force along the opposite direction of ATT as in Figure 4.2.

4.1.1 Parallel PAM Configuration

As shown in Figure 4.2, parallel configuration PAMs are placed in parallel to one another. In every angle of flexion, the length of every PAM and its respective angle along the axis of tibia plate is measured. Figure 4.2 illustrates the brace in 0° and 30° flexion angles.

At 0° flexion, the length of PAM 4 is at its original length. But at 30° , the clamping holes' separation distance reduce and the slackness occurs in the overall length of the PAM. The end points of the PAMs connected to the clamps are considered to be dead lengths and do not add to the preserved length of the PAM. This can be written as:

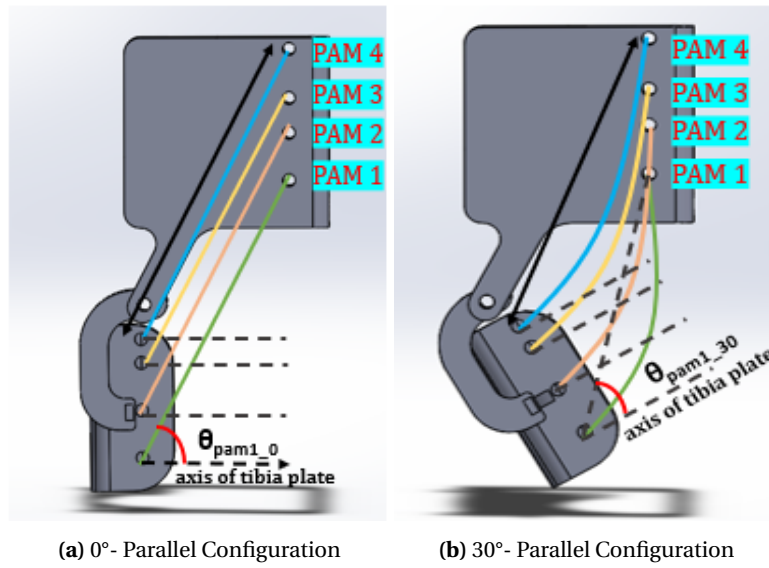


Figure 4.2: Black arrow indicating change in PAM length from 0° to 30° flexion

PAM Preserved length (PL) = Total length (L) - Dead length (L_{dead})

$$\%PL = \frac{PL}{L} * 100 \quad (4.1)$$

Based on the distance between the clamping holes, the length of PAM in parallel configuration is designed to be 200 mm. Only in 0° flexion, the PL is equal to the original or the total length of the PAM. The dead lengths of PAMs 1-4 are 4mm, 4mm, 0mm and 5mm respectively. With this the %preserved length values are calculated as in Table 4.1. The PAM angles, θ_{PAM} , in each of the flexion angles measured are listed in Table 4.1.

Parallel	Total PAM length mm				%Preserved Length				PAM Angle degree			
	0	30	60	90	0	30	60	90	0	30	60	90
Flexion Angle degree												
PAM 1	204	175	134	68	100	85.5	65	32	58	41	23	16
PAM 2	204	184	155	119	100	90	75.5	57.5	58	37	14	-16
PAM 3	200	188	173	154	100	94	86.5	77	56	31	4	-24
PAM 4	205	200	190	177	100	97.5	92.5	86	57	31	4	-30

Table 4.1: PAM placement data in parallel configuration

4.1.2 Crossed PAM Configuration

As the name suggests, crossed configuration consists of PAMs placed in crossed pattern. Unlike in parallel configuration, the body of PAMs traverse over one another when clamped at end points - Figure 4.3. Besides, the length of all PAMs at initial stance is distinct. Therefore, it is necessary to evaluate the factors preserved length and PAM angle for detailed analysis.

The preserved length can be calculated as in Equation 4.1. The lengths of PAMs and corresponding dead lengths are listed in Table 4.2 below.

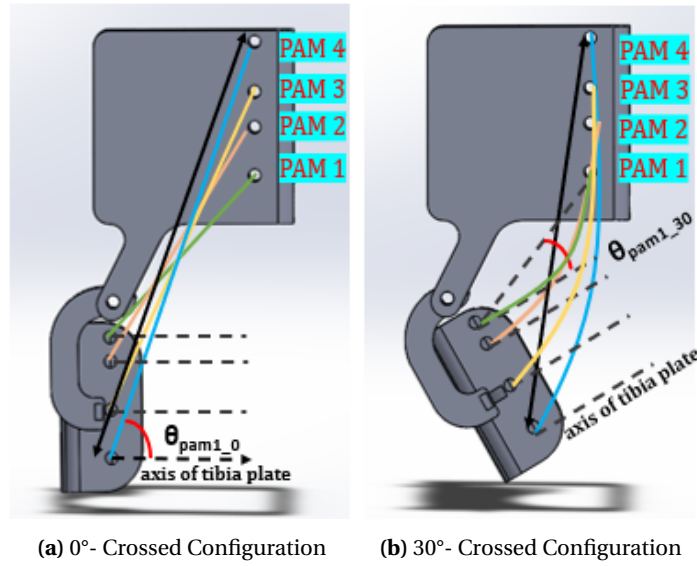


Figure 4.3: Black arrow indicating change in PAM length from 0° to 30° flexion

	Crossed Configuration			
	PAM 1	PAM 2	PAM 3	PAM 4
Total Length (mm)	150	180	230	280
Dead Length (mm)	5	4	4	8

Table 4.2: The varying total length of PAMs in crossed configuration

Crossed	Total PAM length mm				%Preserved Length				PAM Angle degree			
	0	30	60	90	0	30	60	90	0	30	60	90
Flexion Angle degree												
PAM 1	145	137	125	111	100	88.0	80.0	70.7	47	17	9	39
PAM 2	176	166	150	131	100	90.0	81.1	70.6	28	27	1	28
PAM 3	226	208	179	143	100	88.7	76.1	60.4	28	39	15	11
PAM 4	272	248	209	160	100	85.7	71.8	54.3	23	46	24	0.2

Table 4.3: PAM placement data in crossed configuration

4.2 Evaluation of placement configurations

Choice of standard %Preserved length: The standard for preserved length is based on the chosen maximum contraction length in Section 2.4. Since the standard contraction length is 25%, the remaining 75% length is considered to be the standard preserved length. Only the PAMs with percentage preserved length $\geq 75\%$ can be used for actuation.

The data from Table 4.1 and Table 4.3 determines the %preserved lengths available for every angle of flexion. Though PAM angle plays a role in determining the maximum effectiveness of a PAM, a higher PAM angle would not categorize the PAM as non-utilizable. Therefore, as an initial level of filtering, the %preserved lengths are evaluated.

Figure 4.4 represents the tabular data of parallel and crossed configurations in 3D bar graph respectively. The vertical bars represent the percentage length of every PAM at a given flexion angle. The percentage between 0-50% is filled in red, 51-74% in orange and from 75-100% in green. From the color coding, it is convenient to identify the PAMs which can actually contribute to produce force. All the PAMs with surface highlighted in green are categorized to

be *qualified and contributing* at that flexion angle and the surface with other colors are *non-contributing*.

Example: From Table 4.1 and Table 4.3, consider the case 60 deg flexion.

Parallel configuration consists of 3 PAMs namely PAM2, PAM3 and PAM4 whose surface is represented in green meaning that these PAMs are qualified to be activated at 0° flexion. PAM 1's surface being orange means that it is non-contributing. Furthermore, in crossed configuration, PAM1, PAM2 and PAM3 are surfaced in green at 60° flexion meaning that they are qualified while PAM 4 is non-contributing.

Every PAM with %preserved length $\geq 75\%$, qualifies itself to be contributing to ATT recovery force. However, the criteria can only serve as a qualifying factor. In certain flexion angles where all or most of PAMs are $> 75\%$, it is necessary to quantify the forces proportionately using a criterion that is a combination of both %preserved length and the PAM angle. Being one of the primary subjects of this research, the quantification of recovery forces has been discussed in Section 5.6.

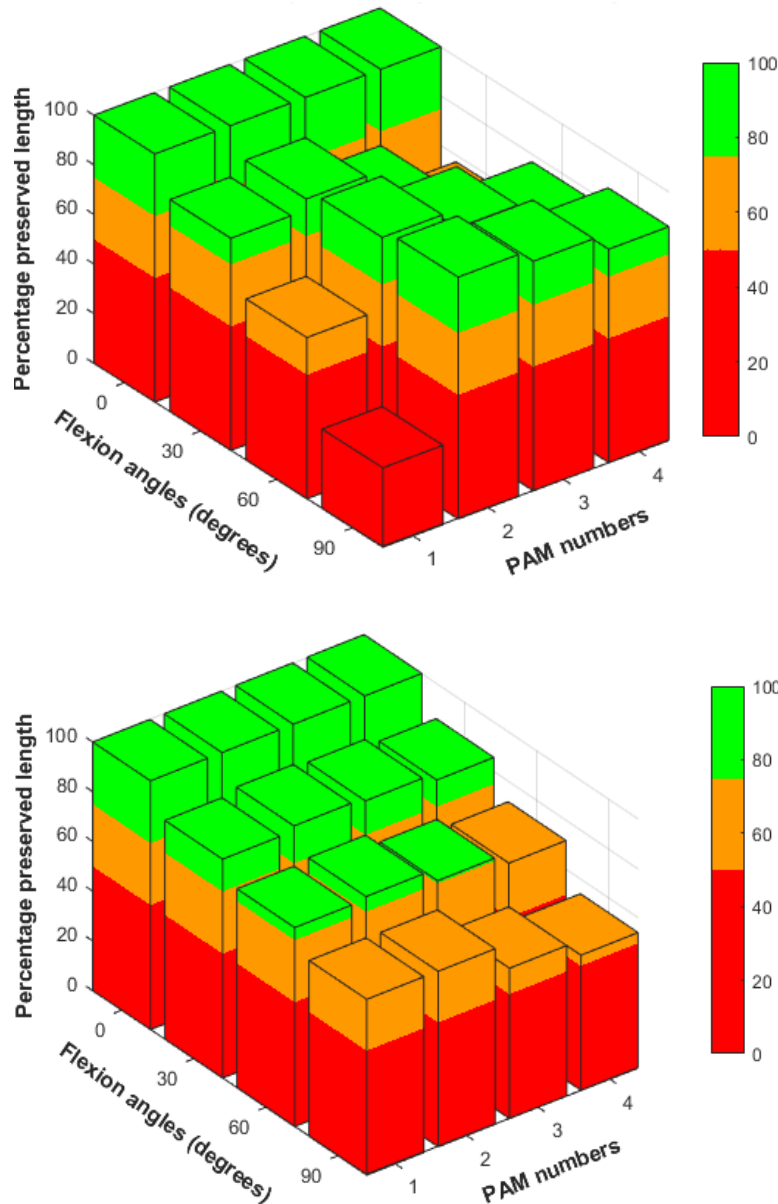


Figure 4.4: Preserved length determining PAM usability in parallel and crossed configuration

5 Simulation

Introduction and Purpose

Concepts discussed in Chapter 3 proposes an overall design of the improved soft-robotic knee brace. The positioning of PAMs on the brace as discussed in Chapter 4 is made such that when activated, the forces exerted by these PAMs would coordinate with the hamstring muscle group to overcome the ATT and ATT in combination with IE in an ACL ruptured knee. The prismatic slider design in the tibial support plate is proposed to mimic the relative sliding motion of the tibia when appropriate stiffness and force parameters are applied.

To verify the performance of the proposed concept of the knee brace, it becomes necessary to model the knee behaviour and then implement the parameters modelled in the brace. To accomplish this, the prismatic slider modelled in the knee brace design is simplified to a 2-link based prismatic joint as in Figure 5.1. The anterior sliding motion of the tibia is simulated through the two-link prismatic joint.

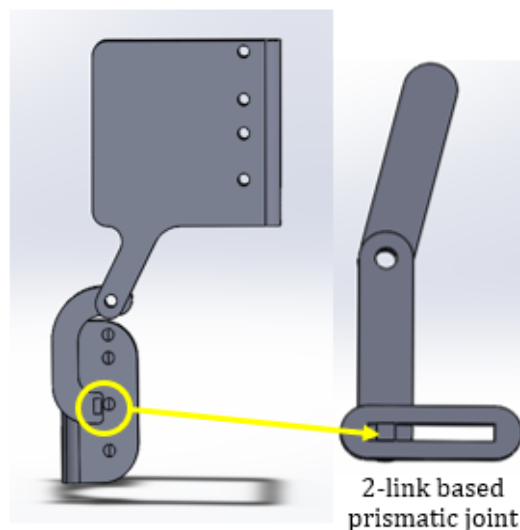


Figure 5.1: Model to estimate pure translation at 0° flexion

5.1 Two-link model of the knee brace

A simplified 3D model of the knee modelled in SolidWorks® was simulated using Simscape Multibody™ - a product of Mathworks [2020]. The Simscape Multibody Link plug-in acts as an interface for exporting the CAD assembly into Simscape Multibody software. The simulation of the model is intended to validate the results obtained in experiments performed by Naghibi et al. [2020]. The intact and ruptured pure ATT values from the experiments are listed in Table 5.1.

Angles in deg	ATT - Intact in mm	ATT - Ruptured in mm
0	-3.57	-27.41
30	-5.19	-36.67
60	-11.55	-44.31
90	-17.97	-52.52

Table 5.1: Pure ATT in intact and ruptured knee values obtained from results

The research focuses on verifying two factors affecting the stability of knee joint as mentioned in Section 2.2. Firstly, the ATT and then the ATT combined with IE. For a thorough sequence of verification, we propose simulation in two phases. Namely:

1. Pure translation discussed under Section 5.2.
2. ATT combined with IE discussed under Section 5.3.

5.2 Pure translation

The context of pure translation means that the ATT is tested in the absence of IE. The displacement of tibia is along its central axis. To simulate this, a 2D model of the knee joint, Figure 5.2, is designed. The model consists of three parts - Fixed femur link (P1), Rotating tibia link (P2), Prismatic Slider (P3) and two joints - Revolute (J1), Prismatic (J2). Simscape equivalent of this model is as shown in Figure 5.4. Individual blocks are explained in Section A.2.

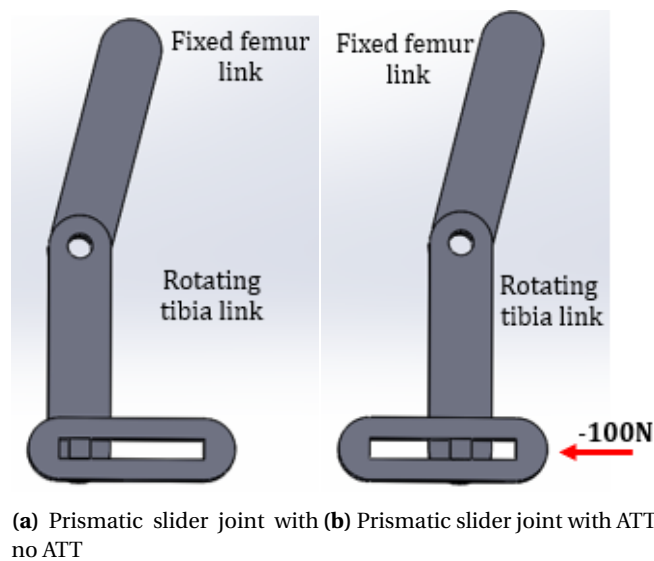


Figure 5.2: Model to estimate pure translation at 0° flexion

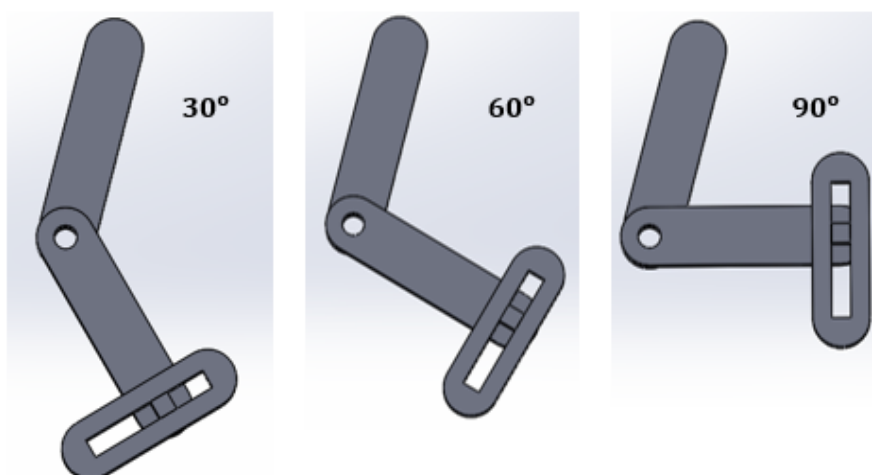


Figure 5.3: Flexion angles 30°, 60° & 90° illustrated in 2-link model

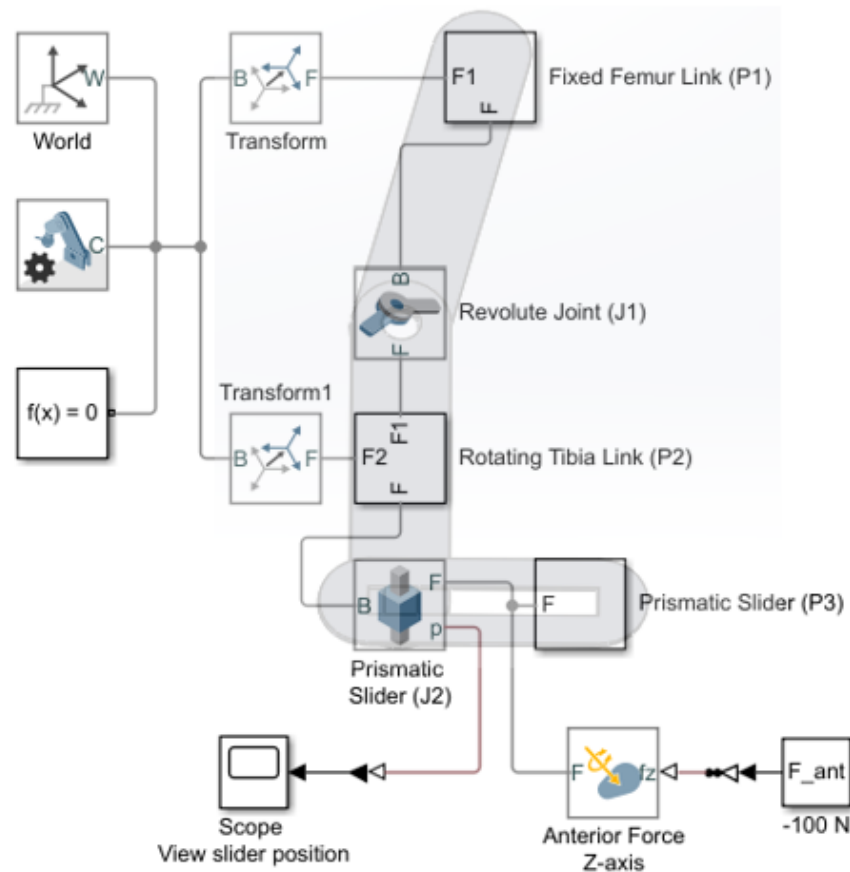


Figure 5.4: Simscape equivalent of Figure 5.2

5.2.1 Model outputs - Pure Translation

The anterior tibial translation can be simulated via the prismatic joint when the appropriate value of stiffness and force acting on the knee during flexion angles is fed to the model. To validate this, the reference values from the experiment were used. The reference experiment provided the ATT at flexion angles 0° , 30° , 60° & 90° as in Table 5.1 when an anterior force of -100N was acting on the tibio-femoral joint. Having known x & F_{ant} , calculated values of K in intact and ruptured knee is calculated in Table 5.2. To load spring stiffness value to the model, it was estimated using Hooke's law:

$$F_{ant} = -Kx \quad (5.1)$$

where x , in this case, is the anterior translation of tibia.

Angles in deg	ATT - Intact in mm	K_intact in N/mm	ATT - Ruptured in mm	K_ruptured in N/mm
0	-3.57	-28.01	-27.41	-3.65
30	-5.19	-19.27	-36.67	-2.73
60	-11.55	-8.66	-44.31	-2.26
90	-17.97	-5.56	-52.52	-1.90

Table 5.2: Stiffness in intact and ruptured conditions - Pure ATT

5.2.2 Choice of damping factor in pure translation

The input values of K and F to the model as in Table 5.2 did not result in the ATT as expected. Figure 5.5 shows the example at 0° flexion where the output translation was observed to be unstable around -3.57 mm indicated by orange line and varying between 0 to -7 mm.

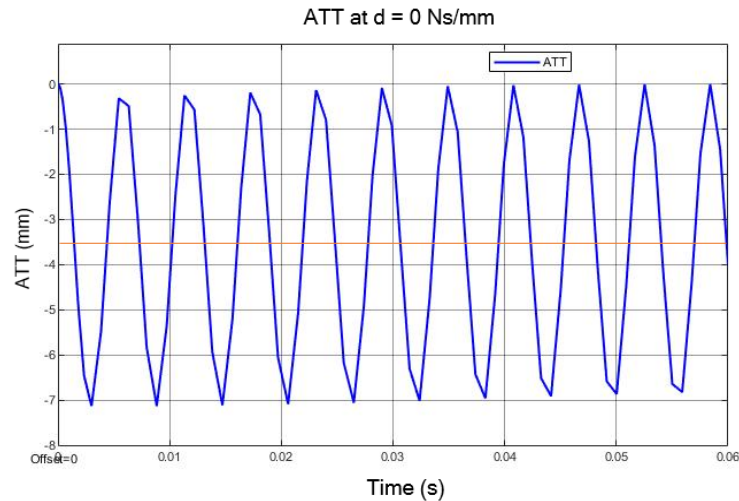


Figure 5.5: Unstable ATT fluctuating around -3.57 mm (orange line) at 0° flexion with damping factor = 0 Ns/mm from Table 5.2

With detailed inspection, it was found that the ATT was dependent on the damping factor of the joint. To stabilize the translation, the damping factor had to be decided for all the trials including intact and ruptured conditions. The damping factor was gradually increased in steps of 0.01 and the difference was observed as in Figure 5.6

The overshoot of the curve was observed until damping ratio of 0.04 Ns/mm. Beyond this value, the response was settled. The simulations in Figure 5.6 is illustrated for the case of 0° flexion where the calculated ATT was -3.57 mm. For the rest of the trials involving flexion angles 30 , 60 & 90° flexion the damping factor of 0.05 Ns/mm was retained. Beyond the value of 0.05 Ns/mm, the response was observed to be overdamped.

5.3 ATT combined with IE

Pure translation, as mentioned in Section 5.2, refers to the translation of tibial bone along the central axis. In presence of internal-external rotation of tibia, the translation is no longer the centre line but along either sides of the central axis. In order to study this effect, two parallel links as in Figure 5.7 was used instead of one. With the addition of second link, it was intended to study the ATT along medial and lateral sides of the joint simultaneously defined as *Representative translations* in medial and lateral sides.

Firstly, to obtain the medial and lateral representative translations, an internal rotation was applied to the pure translation values listed under Section 5.2. The values of IE rotation was from the reference experimental results listed in Table 5.3 with its pure translation and translation combined with rotation in ruptured ACL condition.

Since pure translation occurs along the central axis and medial and lateral representative translations along the either ends of the tibia (Figure 5.8), it becomes necessary to assume the overall width of tibia to calculate these translations. However, in this research, the width of the tibial plate of the knee brace (Figure 5.7) has been used instead of the width of tibia itself considering the fact that the forces are applied along either sides of tibia support plate. By combining the data of pure translation, IE rotation and the width of tibia plate, medial and lateral representative translation (T_{med} & T_{lat}) can be calculated as explained below.

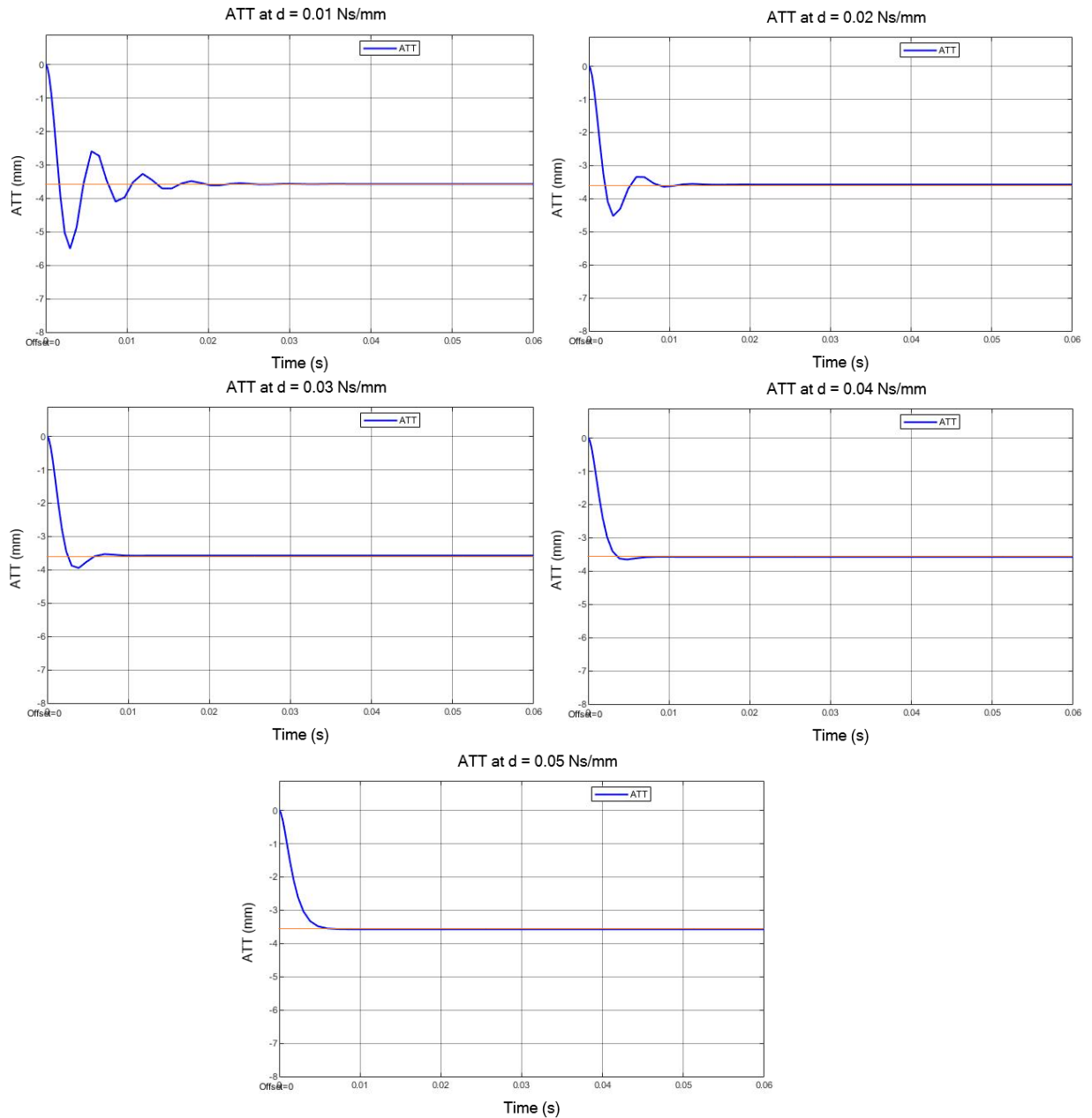


Figure 5.6: ATT observed at 0° flexion for damping factors from 0.01 Ns/mm to 0.05 Ns/mm (left to right) respectively

Angles degrees	ATT - Intact mm	IE Rotation - intact degrees	ATT - Ruptured mm	IE Rotation - ruptured degrees
0	-3.57	2.7	-27.41	13.8
30	-5.19	-0.4	-36.67	8.6
60	-11.55	-5.1	-44.31	2.7
90	-17.97	-6.5	-52.52	0.4

Table 5.3: IE Rotation observed in intact and ruptured ACL knees from previous experimental results

1. From the 3D model of the tibia plate, distance between plates, $W = 83$ mm
2. Pure translation of intact knee at 0° flexion, $T_{int0} = -3.57$ mm

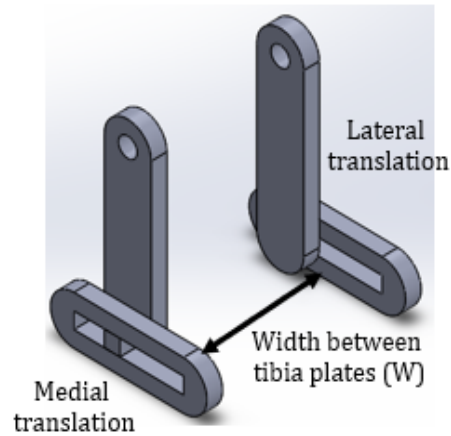


Figure 5.7: 3D model to study medial and lateral representative translation

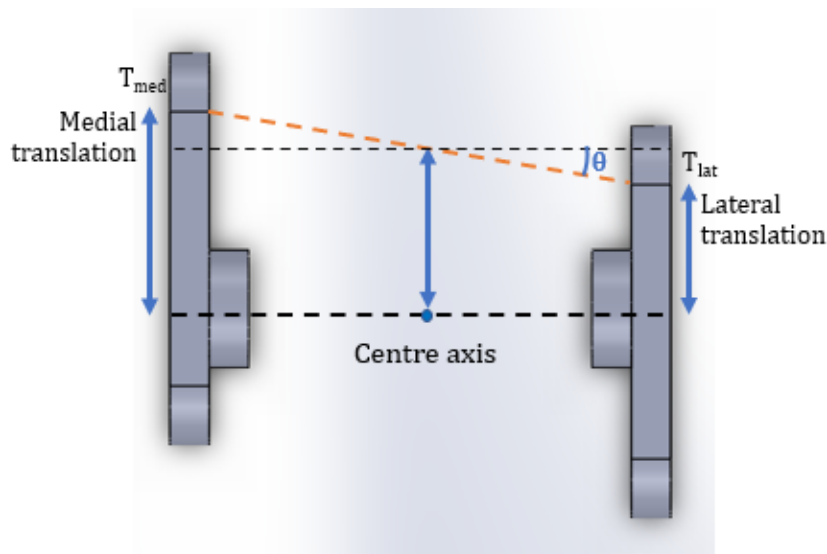


Figure 5.8: Tibial plates with medial and lateral representative translation

3. IE rotation of intact knee at 0° flexion, $R_{int0} = 2.7^\circ$

Difference from centre axis,

$$\begin{aligned} \mathbf{T}_{\text{difference}} &= (W/2) * \tan(R_{int0}) \\ \mathbf{T}_{\text{difference}} &= -1.957\text{mm} \end{aligned}$$

Medial and lateral representative translations,

$$\begin{aligned} \mathbf{T}_{\text{med}} &= \mathbf{T}_{\text{int0}} - \mathbf{T}_{\text{difference}} = -1.63\text{mm} \\ \mathbf{T}_{\text{lat}} &= \mathbf{T}_{\text{int0}} + \mathbf{T}_{\text{difference}} = -5.50\text{mm} \end{aligned}$$

To estimate the medial and lateral representative translation for the rest of the trials in intact and ruptured conditions, the behaviour was estimated using AppDesigner. The corresponding medial and lateral representative translations are shown in Table 5.4 and Table 5.5.

5.3.1 Model Outputs - ATT combined with IE

The parameters to be fed into the model to simulate medial and lateral representative translation differs than in pure translation. The anterior force acting on the knee being -100 N gets

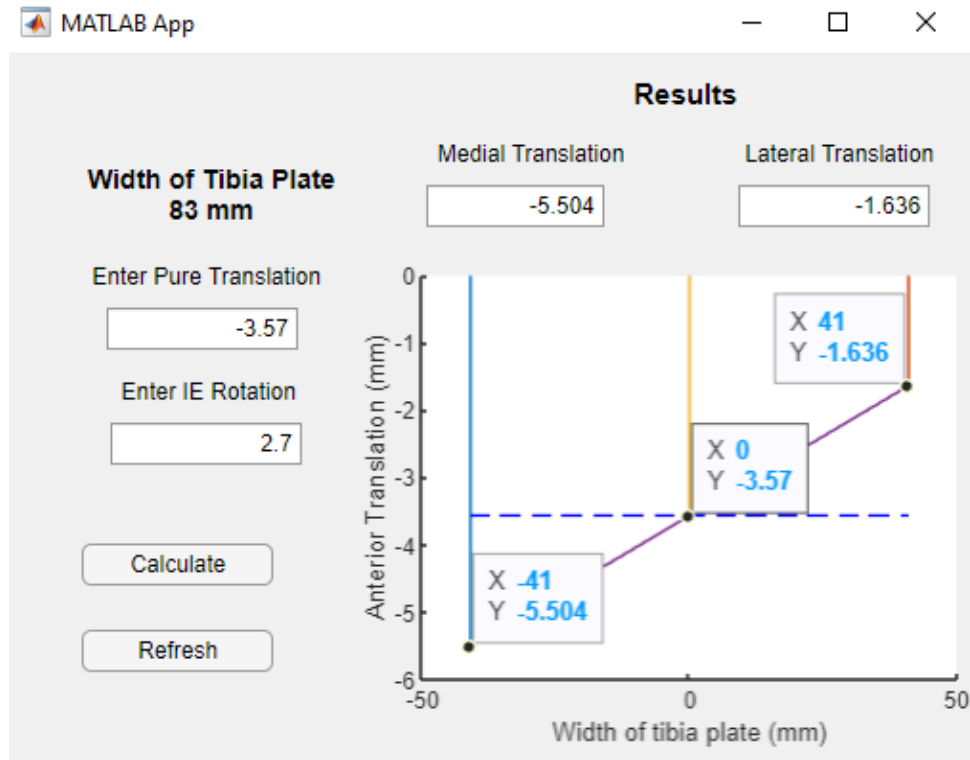


Figure 5.9: Medial and Lateral representative translations plotted by providing input to GUI in AppDesigner

Flexion Angle degree	Translation - Intact knee mm		
	Pure	Medial representative	Lateral representative
0	-3.57	-5.50	-1.64
30	-5.19	-4.90	-5.48
60	-11.55	-7.89	-15.21
90	-17.97	-13.30	-22.64

Table 5.4: Medial and lateral representative translations in the intact knee

Flexion Angle degree	Translation - Ruptured knee mm		
	Pure	Medial representative	Lateral representative
0	-27.41	-37.48	-17.34
30	-36.67	-42.87	-30.47
60	-44.31	-46.24	-42.38
90	-52.52	-52.81	-52.23

Table 5.5: Medial and lateral translations in the ruptured knee

divided in the joint to cause medial and lateral representative translation. Equation 5.1 can now be rewritten as

$$F_{ant} = F_{ant_med} + F_{ant_lat} \quad (5.2)$$

$$F_{ant} = -(K_{med} * x_{med} + K_{lat} * x_{lat})$$

Deciding if the division of force would be proportional according to the ATT or if it would be divided equally regardless is perhaps an interesting subject of research. The joint laxity discussed under Section 2.2.2 mentions that the lateral surface has a higher variation than medial as the medial is more firmly anchored than the lateral meniscus providing mobility against its restraining ligaments. Thus, when force is applied on the joint, the difference in stiffness due to morphological variations and also due to the stiffness of cruciate ligaments causes different translations. The difference in translation gives rise to an internal or external rotation of tibia.

Considering that the total ATT depends on the stiffness in the joint, the force was chosen to be acting equally on either side. If a proportional distribution of force was chosen, the corresponding proportional increase or decrease in translation would lead to extremely high or low values of stiffness. Therefore, the values of medial and lateral anterior force F_{ant_med} & F_{ant_lat} are considered -50 N each in further context. Table 5.6 contains calculated medial and lateral stiffness K_{med} & K_{lat} in intact and ruptured conditions.

Stiffness	Intact N/mm		Ruptured N/mm	
	Medial	Lateral	Medial	Lateral
Flexion Angle degree				
0	-9.09	-10.2	-6.34	-3.76
30	-30.55	-9.13	-3.29	-2.21
60	-1.33	-1.17	-1.08	-0.95
90	-2.88	-1.64	-1.18	-0.96

Table 5.6: Medial and lateral stiffness calculated at medial and lateral anterior force equal to -50 N each

5.3.2 Choice of damping factor in ATT combined with IE

The experiment under Section 5.2.2 tested for damping factors ranging between 0 to 0.05 and a final damping value of 0.05 was chosen to be optimal. A similar approach was followed in this section. By observing Table 5.6, the value of K ranges between -0.957 (min) to -30.555 (max). Following were the inferences when selecting the damping factor as in Figure 5.10:

- For lower values of stiffness, less than 25 N/mm, the damping factor of 0.05 yielded required ATT.
- For stiffness beyond 25 N/mm, overshoot in the ATT was observed. Therefore, the damping factor was further increased from 0.05 N/mm.
- Though the curve settled at 0.07, smoother transition was observed at damping factor 0.08.

However, damping factor of the model cannot vary in every trial since the damping of knee remains a single value for every individual. The variation of damping value is dependent on the activity being carried out. For different loading forces acting on the knee, the damping factor changes as discussed in Dutto and Smith [2002] and Schneider et al. [2017]. This necessitated to use a single damping factor for all trials: Pure translation, Medial-Lateral representative translation of intact and ruptured knee.

Choice made: Besides yielding satisfying results for higher values of stiffness (beyond 25 N/mm), the damping factor of 0.08 also produced satisfactory ATT also for lower values of stiffness (less than 25 N/mm). Hence, final value of damping was chosen 0.08 Ns/mm. Table provides a comparison of ATT in experimental and simulation cases.

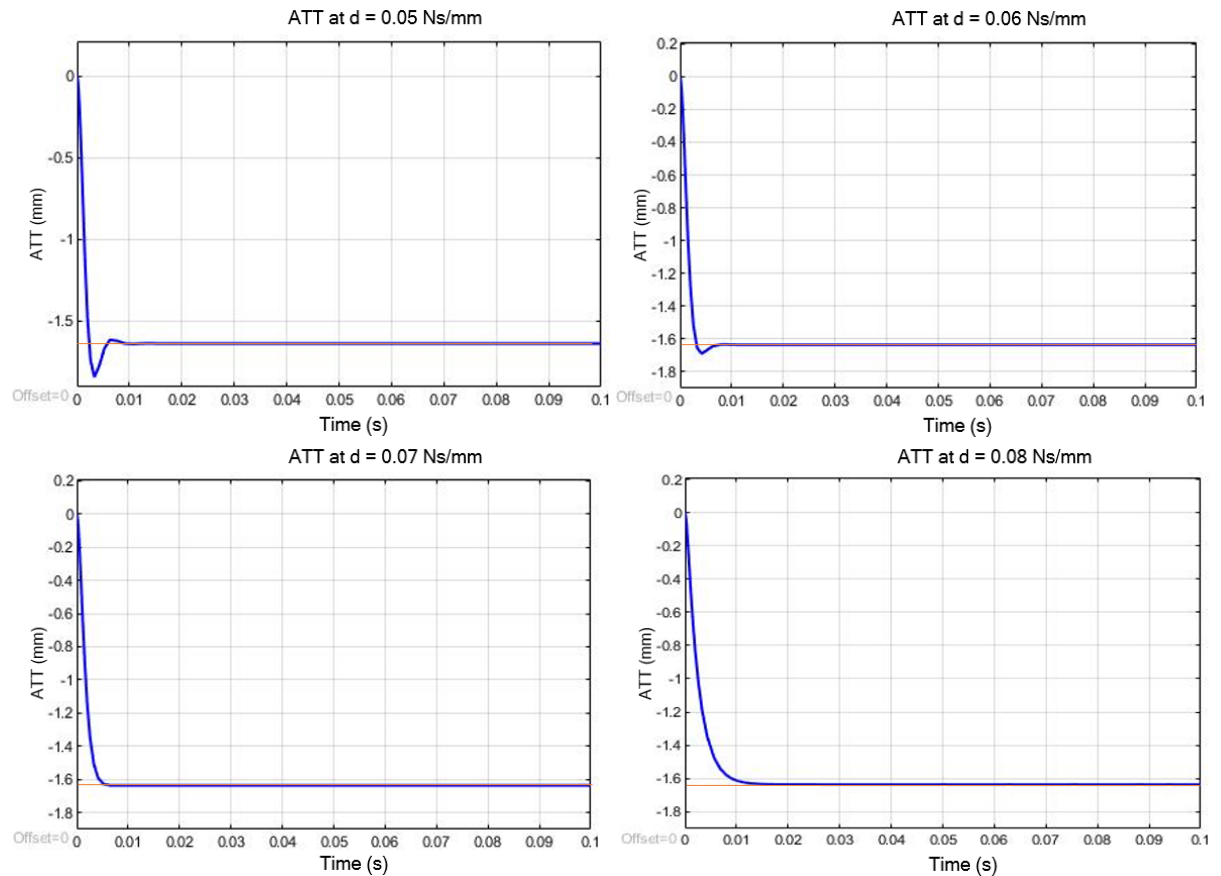


Figure 5.10: Lateral representative ATT (-1.64 mm) observed when (high) stiffness, $K = 30.55$ for damping factors from 0.05 Ns/mm to 0.08 Ns/mm at 30° flexion

Intact D = 0.08 Ns/mm	Stiffness N/mm		ATT - Medial Representative (mm)		ATT - Lateral Representative (mm)	
	Medial	Lateral	Experimental	Simulation	Experimental	Simulation
Flexion Angle degree						
0	-9.09	-30.55	-5.50	-5.50	-1.64	-1.64
30	-10.20	-9.13	-4.90	-4.90	-5.48	-5.48
60	-6.34	-3.29	-7.89	-7.89	-15.21	-15.21
90	-3.76	-2.21	-13.30	-13.30	-22.64	-22.64

Table 5.7: Measured values of intact knee ATT with damping factor = 0.08 Ns/mm

Ruptured D = 0.08 Ns/mm	Stiffness N/mm		ATT - Medial Representative (mm)		ATT - Lateral Representative (mm)	
	Medial	Lateral	Experimental	Simulation	Experimental	Simulation
Flexion Angle degree						
0	-1.33	-2.88	-37.48	-37.47	-17.34	-17.34
30	-1.17	-1.64	-42.87	-42.84	-30.47	-30.47
60	-1.08	-1.18	-46.24	-46.19	-42.38	-42.35
90	-0.95	-0.96	-52.81	-52.67	-52.23	-52.10

Table 5.8: Measured values of ruptured knee ATT with damping factor = 0.08 Ns/mm

Flexion Angle degree	Stiffness N/mm	Pure ATT - Ruptured(mm)	
		Experimental	Simulation
0	-28.01	-3.57	-3.57
30	-19.27	-5.19	-5.11
60	-8.66	-11.55	-11.55
90	-5.56	-17.97	-17.97

Table 5.9: Measured values of intact knee's pure ATT with damping factor = 0.08 Ns/mm

Flexion Angle degree	Stiffness N/mm	Pure ATT - Ruptured (mm)	
		Experimental	Simulation
0	-3.65	-27.41	-27.41
30	-2.73	-36.67	-36.63
60	-2.26	-44.31	-44.17
90	-1.90	-52.52	-52.08

Table 5.10: Measured values of ruptured knee's pure ATT with damping factor = 0.08 Ns/mm

Since a constant damping factor has to be maintained and the results with pure translation at 100 N had a damping factor of 0.05 Ns/mm, the model had to be re-tested with the new damping factor 0.08 Ns/mm. Table 5.9 and Table 5.10 shows pure translation of intact and ruptured knee with anterior force = -100 N and damping factor = 0.08 Ns/mm. The experimental and simulated ATT values suggests that the new damping factor does not cause much of difference when compared.

5.4 ATT Recovery Force - F_{rec}

The simulation of models in Section 5.2 and Section 5.3 results in intact and ruptured knee ATT values with pure translation and ATT combined with IE. By the fixation of multiple PAMs along medial and lateral sides of the robotic knee brace, the ATT of ruptured knee is intended to be recovered back to the ATT as in an ACL intact knee. To implement this, a force opposite in the direction of ATT must act upon the knee. The force in this case is regarded as the force of PAMs that act according to the alignment criteria namely the preserved length and fixation angle as discussed in Section 4.1. Every PAM is designed to produce a maximum force of 50 N at a pressure of 2 bars. By using all the PAMs that are available to be used in a given angle of flexion, a total force, F_{PAM} , must be produced that corrects the ATT from ruptured state to the ATT in intact state.

From the Simscape model in Figure 5.4, the F_{ant} block produces force acting in the anterior direction (F_{ant}) thus causing ATT. To recover this, another force block F_{rec} acting in the direction opposite to ATT is added. F_{rec} is the summation of forces of available PAMs in every flexion angle. F_{ant} and F_{rec} are constants loaded from MATLAB's workspace. Figure A.3 shows the equivalent model in Simscape with medial and lateral representative translation with corresponding F_{ant} and F_{rec} .

From Figure 5.11, force acting on knee, F_{ant} is -100 N. By providing the ruptured knee stiffness values to the model, ATT is simulated. Consider the case at 0° flexion from Table 5.2 where the ruptured knee ATT is -27.41 mm with a stiffness of -3.6 N/mm. However, ideally the ATT is supposed to be -3.57 mm by retaining the ruptured knee stiffness. Through F_{rec} block, force is varied from 0 N to a value where the ATT was no longer -27.41 mm but -3.57 mm. Hence the

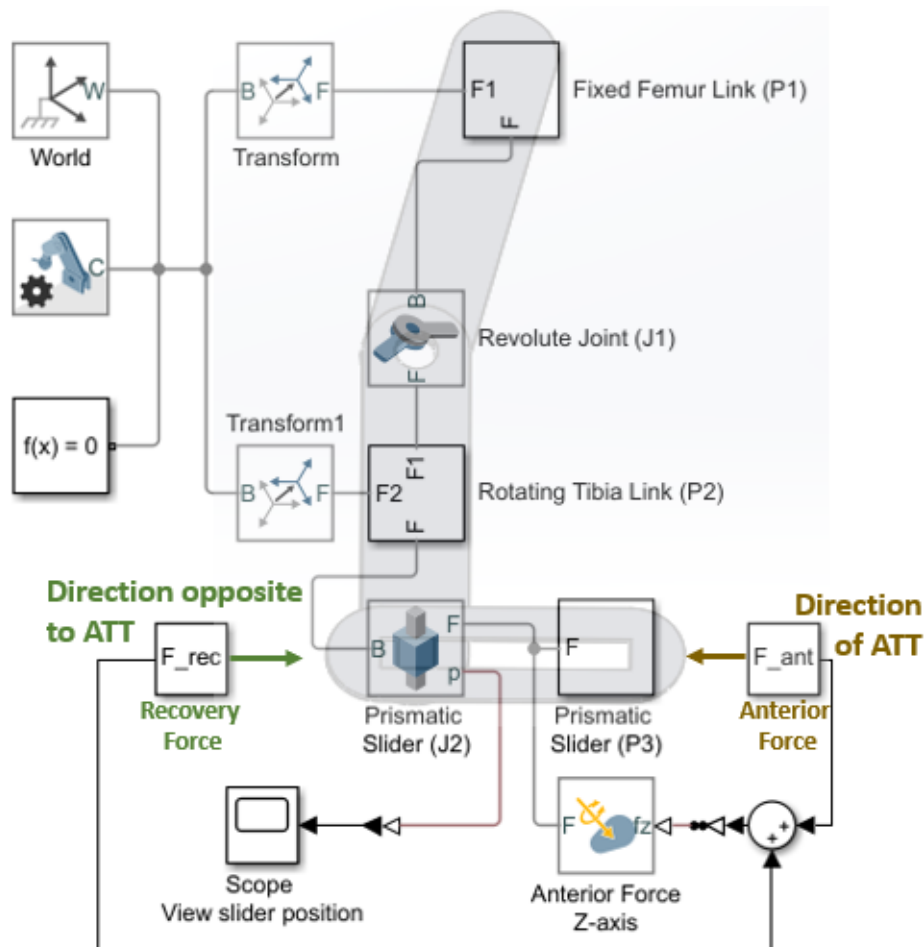


Figure 5.11: Simscape model for pure translation with anterior force - F_{ant} and recovery force F_{rec}

opposite force in this case is found to be 87 N. Table 5.11 contains the values of recovery force for ruptured knee with pure translation between 0° and 90° flexion.

Flexion Angle degree	Stiffness N/mm	Pure - ATT (mm)		Recovery Force N
		Intact	Ruptured	
0	-3.65	-3.57	-27.41	87
30	-2.73	-5.19	-36.67	85.85
60	-2.26	-11.55	-44.31	74
90	-1.90	-17.97	-52.52	65.78

Table 5.11: Recovery force measured for ruptured knee with pure translation between 0° and 90° flexion

Similarly, Table 5.12 and Table 5.13 contains the values of F_{rec} for ruptured knee with medial and lateral representative translation between 0° and 90° flexion.

Flexion Angle degree	Stiffness N/mm	ATT - Medial Repr. (mm)		Recovery Force N
		Intact	Ruptured	
0	-1.33	-5.50	-37.48	42.66
30	-1.17	-4.90	-42.87	44.28
60	-1.08	-7.89	-46.24	41.5
90	-0.95	-13.30	-52.81	37.38

Table 5.12: Recovery force measured for ruptured knee with medial representative translation between 0° and 90° flexion

Flexion Angle degree	Stiffness N/mm	ATT - Lateral Repr.(mm)		Recovery Force N
		Intact	Ruptured	
0	-2.88	-1.64	-17.34	45.3
30	-1.64	-5.48	-30.47	41.02
60	-1.18	-15.21	-42.38	32.06
90	-0.96	-22.64	-52.23	28.28

Table 5.13: Recovery force measured for ruptured knee with lateral representative translation between 0° and 90° flexion

5.5 Division of PAM forces

The total forces from the PAM results in F_{PAM} as discussed under Section 5.4. However, the division of force between the PAMs 1 to 4 is purely dependent on the placement layout of these PAMs. Section 4.1 discusses two configurations to decide which one of the two qualifies to perform in all the 4 angles of flexion. Based on the two selection criteria, angle of placement and preserved length, each PAM characterizes itself to its unique maximum level of actuation in every flexion angle. This individual value of PAM characterization is the **Weighting Factor**. Depending on the weighting factors of every PAM in each flexion angle, the controller decides a proportion to divide the forces.

Among the two configurations (parallel and crossed) in Section 4.1, the weighting factor has been estimated for parallel and crossed configurations. From values in Table 4.1 and Table 4.3, the weighting factor can be estimated as shown below:

$$WF = \cos(\theta) * PL \quad (5.3)$$

where θ is the angle of placement of PAMs, PL is the percentage of preserved length.

Table 5.14 represents the $\cos(\theta)$ and Table 5.15 represents the preserved length (PL) respectively. Table 5.16 is the weighting factor estimated from Equation 5.3.

5.5.1 Parallel Configuration

Referring to Table 5.16, the numbers indicated in brackets next to weighting factors indicate the priority. The priority varying from scale 1 to 4 means that the PAM with priority 1 has the highest weighting factor and ranges until 4, with 4 being the lowest priority.

Explaining Table 5.16:

Case I: Pure translation with recovery force, $F_{rec} = 87$ N at 0° flexion (Table 5.11)

- PAM3 has the highest weighting factor of 0.559 with priority 1, PAM4 gets the second priority while 3rd, 4th PAMs have the last priority.

Criteria 1 - Cosine(PAM angle)				
Flexion Angle degree	0	30	60	90
PAM 1	0.530	0.755	0.921	0.961
PAM 2	0.530	0.799	0.970	0.961
PAM 3	0.559	0.857	0.998	0.914
PAM 4	0.545	0.857	0.998	0.866

Table 5.14: Criteria 1 showing cosine of PAM placement angles from Table 4.1

Criteria 2 - %Preserved Length				
Flexion Angle degree	0	30	60	90
PAM 1	100	85.5	65	32
PAM 2	100	90	75.5	57.5
PAM 3	100	94	86.5	77
PAM 4	100	97.5	92.5	86

Table 5.15: Criteria 2 showing %preserved lengths as in Table 4.1

Parallel Configuration	Weighting Factor Criteria 1 * Criteria 2				Priority	
	0	30	60	90		
PAM 1	0.530 (3)	0.645 (4)	0.598	0.308	1	Highest
PAM 2	0.530 (3)	0.719 (3)	0.733 (3)	0.553	4	Lowest
PAM 3	0.559 (1)	0.806 (2)	0.863 (2)	0.703 (2)		
PAM 4	0.545 (2)	0.836 (1)	0.923 (1)	0.745 (1)		

Table 5.16: Weighting factor as a product of Table 5.14 and Table 5.15 values

- The highest proportion of force thus gets assigned to PAM1.

Case 2: Medial representative translation with medial recovery force, $F_{rec} = 41.5$ N at 60 °flexion (Table 5.12)

- PAM4 has the highest weighting factor of 0.923 with priority 1, PAM3 gets the second priority and PAM2 the least.
- It has to be noted that due to the criteria - 1, %preserved length being < 75%, PAM1 is excluded from contributing to the medial recovery force of 41.5 N. Thus there is no priority assigned to PAM1.
- Therefore, medial recovery force is constituted from PAMs 2,3 & 4

Case 3: Lateral representative translation with lateral recovery force, $F_{rec} = 28.2$ N at 90 °flexion (Table 5.13)

- PAM4 has the highest weighting factor of 0.745 with priority 1, PAM3 gets the second priority.
- Again, as per criteria - 1, the %preserved length for PAMs 1&2 is < 75%. Thus, these PAMs are represented in red and do not contribute to lateral recovery force.
- Therefore, lateral recovery force is constituted from PAMs 2,3 & 4

5.5.2 Crossed Configuration

Similar to the criteria applied in Table 5.16 in parallel configuration. The weighting factor for crossed configuration is shown in Table 5.17. The priority values in case of crossed configuration are assigned upto 60° flexion. From Table 4.3, it is understood that at 90° flexion no PAMs are available to contribute as their preserved lengths are lesser than the required 75% standard. Therefore, assigning priorities to these PAMs are not considered.

Crossed Configuration	Weighting Factor Criteria 1 * Criteria 2				Priority	
	Flexion Angle	0	30	60	90	
PAM 1	0.682 (3)	0.842 (1)	0.790	0.549	1	Highest
PAM 2	0.883 (2)	0.802 (2)	0.811 (1)	0.623	4	Lowest
PAM 3	0.883 (2)	0.689 (3)	0.735 (2)	0.593		
PAM 4	0.921 (1)	0.595 (4)	0.656	0.543		

Table 5.17: Weighting factor in the crossed configuration

5.6 Quantification of recovery forces

Above section explains how weighting factor plays the role in dividing the forces to be assigned to PAMs. However, with the weighting factor, it is only possible to know the proportion in which the force can be divided. It is necessary to implement a logic with which the controller quantifies the precise amount of force that should be assigned to each PAM. At every flexion angle, the total recovery forces, medial recovery force and lateral recovery force are listed in Table 5.11, Table 5.12 and Table 5.13 respectively. Note that the recovery force in the equations is a generic representation irrespective of pure, medial or lateral force. Recovery force (F_{rec}) represented in Equation 5.5 corresponds to the F_{rec} block in the Simscape model in Figure 5.11.

The equations below calculate the PAM forces in a given flexion angle based on the weighting factors in Table 5.16. The force factor to calculate recovery force is based on the normalization of weighting factors. i refers to the PAM number ranging up to j . With W_{norm} as the normalized value of weighting factors,

$$W_{norm}(i) = \frac{W(i)}{\sum_{i=1}^j \sqrt{W(i)^2}} \quad (5.4)$$

$$f_{factor} = \frac{F_{rec}}{\sum_{i=1}^j W_{norm}(i)} \quad (5.5)$$

f_{factor} refers to the force factor that determines the quantity of force that is contributed by each PAM, $f_{rec(i)}$, in the direction of ATT.

$$f_{rec}(i) = W_{norm}(i) * f_{factor} \quad (5.6)$$

To calculate the force produced by the individual PAM, the angle values can be estimated from Table 5.14.

$$f_{pam}(i) = \frac{f_{rec}(i)}{\cos(\theta_i)} \quad (5.7)$$

The summation of individual recovery forces, $f_{rec}(i)$, accounts to the total recovery force, F_{rec} , acting in opposite direction of ATT in a given flexion angle as in Figure 5.12. Similarly, individual PAM forces, $f_{pam}(i)$, in a given flexion angle sums to the total PAM force, F_{PAM} . The summation is constituted by the forces contributed by the qualified PAMs.

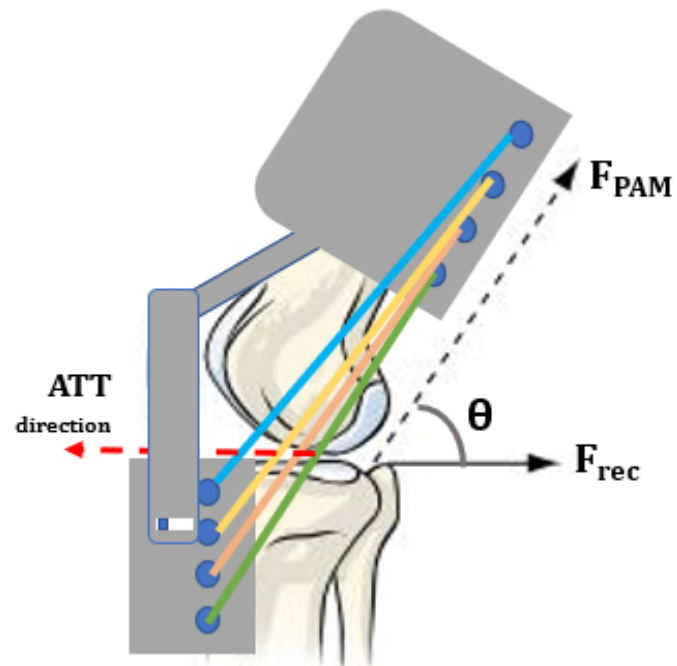


Figure 5.12: Illustration of recovery and PAM forces based on the representation in Xergia et al. [2018]

6 Results and Discussion

This chapter presents the results of experiments conducted. The data from recovery force models simulated under Chapter 5 is presented. The results comprise of Recovery, PAM forces and force distribution. Finally, the calculated recovery force is verified using finite element model and compared with the intact knee conditions.

The Simscape model was tested to reproduce experimental ATT values in pure translation and translation combined with rotation for intact and ruptured ACL knee. To tune for a consistent output, the model was tested under different damping factors. As discussed under Section 5.3.2, a common damping factor 0.08 was set throughout the simulations.

6.1 Recovery Forces - F_{rec}

1. Pure Translation - ACL ruptured knee with anterior force, $F_{ant} = -100$ N

Recovery force is exerted to correct the undesired anterior translation of tibia. Observing pure translation data, the ATT increases as the angle of flexion increases. Thus, at lower angles of flexion, say at 0° & 30° , the recovery force is of higher magnitude (see Figure 6.1). The anterior and recovery force acting opposite to one another results in a sum lesser than the sum of these forces at 60° & 90° flexion angles. In case of pure translation, the force acts along the central axis of tibia which in this research is considered as the axis of rotation.

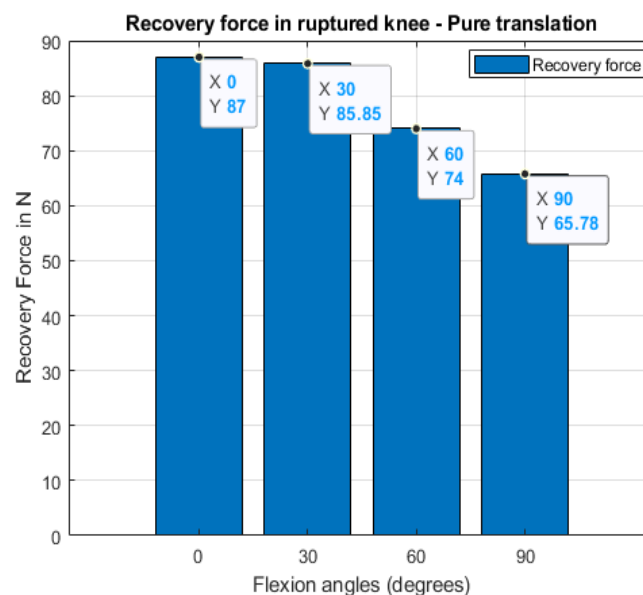


Figure 6.1: Bar graph illustrating the magnitude of recovery force required in pure translation

2. ATT combined with IE - ACL ruptured knee with medial and lateral representative translation

In case of translation that occurs with rotation, though the anterior force gets divided equally towards medial and lateral ends of the tibia. However due to unequal stiffness occurring at the joint because of the loss of ACL and its corresponding effect on the joint laxity, the translation along medial and lateral sides differ. This requires unequal distribution of recovery force to correct the effect. From Figure 6.2, the recovery force at every flexion angle is represented in two blocks namely medial and lateral force. Unlike the anterior medial and lateral forces, corresponding recovery forces vary. However, the sum

of the two forces is observed to be the same as the total recovery force in pure ATT of ACL ruptured knee. This is also evident from the bars in Figure 6.1 and Figure 6.2.

Summation of medial and lateral recovery forces yielded the theoretical sum of recovery force which when compared with the recovery force under pure translation resulted in a similar force. The values have been compared in Table 6.1.

Flexion Angle degree	Recovery Force (N)	
	Pure Translation	Medial + Lateral
0	87	87.96
30	85.85	85.3
60	74	73.56
90	65.78	65.66

Table 6.1: Comparison of total recovery forces

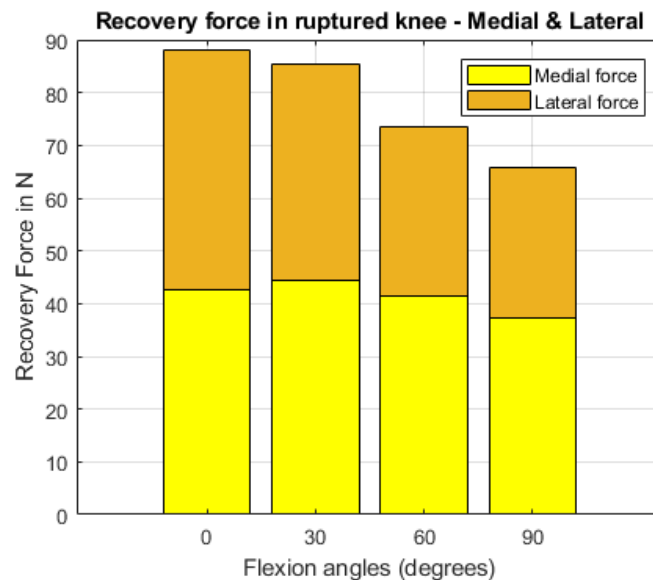


Figure 6.2: Bar graph illustrating the magnitude of recovery force required in medial & lateral representative translation

6.2 Quantification of PAM and Recovery forces

Choice of number of PAMs:

The research focuses on division of forces between four PAMs. The design is made in such a way to have atleast one contributing PAM in every angle of flexion. To avoid the overloading on a single PAM, it is further improvised to multiple PAMs at every flexion angle - although at lower loads, a single PAM can still suffice. Reducing the number of PAMs lesser than four not only constrains the load sharing ability but also causes limitations based on the PAM placement angle and preserved length.

The method to estimate the PAM forces and corresponding recovery force was mentioned under Section 5.6. Table 6.2 shows results from the code calculating the distribution of medial recovery forces and Table 6.3 calculating the distribution of medial PAM forces.

The distribution of total PAM force into individual forces of PAM is illustrated in Figure 6.3. The color coding of PAMs shows the contributing PAMs. Maximum number of PAMs, PAM 1-4, are able to contribute at 0° flexion while at 90° flexion, PAM 3,4 are contributing.

Flexion Angle degree	Medial Recovery Force (N)				
	PAM 1	PAM 2	PAM 3	PAM 4	Sum
0	10.29	10.29	10.85	10.57	42.00
30	9.27	11.04	11.85	11.85	44.00
60	0.00	11.82	14.59	14.59	41.00
90	0.00	0.00	18.88	18.12	37.00

Table 6.2: Calculated values of medial recovery force distribution

Flexion Angle degree	Medial PAM Force (N)				
	PAM 1	PAM 2	PAM 3	PAM 4	Sum
0	19.41	19.41	19.41	19.41	77.65
30	12.28	13.82	13.82	13.82	53.74
60	0.00	12.19	14.62	14.62	41.43
90	0.00	0.00	20.66	20.93	41.59

Table 6.3: Calculated values of medial PAM force distribution

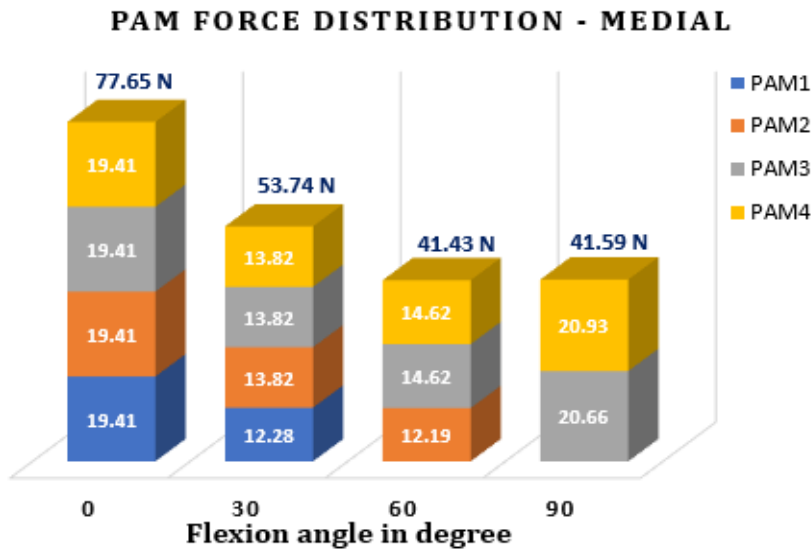


Figure 6.3: Distribution of total PAM forces in medial side

Similarly, the recovery force and PAM force are calculated in Table 6.4, Table 6.5 and its graphical representation of lateral PAM force distribution is illustrated in Figure 6.4. Since the layout of placement of PAMs along the medial and lateral sides is the same, the number of PAMs that are contributing in every flexion angle remains the same but the distribution of forces differ along the either sides.

Discussion in Section 4.2 provides information about availability of PAMs under a given flexion angle based on the criteria of preserved length. If a PAM fails to meet the minimum preserved length of 75% at any angle of flexion, then the PAM is *non-contributing*. Though the preserved length itself is not the only criteria that evaluates the performance of PAM, it can be a qualifying factor to decide if at all the PAM is eligible to contribute. Based on this factor, it was evident from Figure 4.4 that the parallel configuration has contributing PAMs in all flexion angles while crossed configuration has PAMs that can contribute in flexion angles 0°, 30° and 60°.

Flexion Angle degree	Lateral Recovery Force (N)				
	PAM 1	PAM 2	PAM 3	PAM 4	Sum
0	11.02	11.02	11.63	11.33	45.00
30	8.64	10.29	11.04	11.04	41.02
60	0.00	9.25	11.41	11.41	32.06
90	0.00	0.00	14.43	13.85	28.28

Table 6.4: Calculated values of lateral recovery force distribution

Flexion Angle degree	Lateral PAM Force (N)				
	PAM 1	PAM 2	PAM 3	PAM 4	Sum
0	20.80	20.80	20.80	20.80	83.19
30	11.45	12.88	12.88	12.88	50.10
60	0.00	9.53	11.43	11.43	32.40
90	0.00	0.00	15.79	15.99	31.79

Table 6.5: Calculated values of lateral PAM force distribution

Considering the scope of this research, the ATT is intended to be corrected in flexion angles 0°, 30°, 60° and 90°. This limits the consideration of crossed configuration to provide the quantified PAM forces at 90° flexion. Besides, the crossing of PAMs adds to its limitations from the perspective of wearability. However, crossed configuration can only be a subject of comparison if the activity of knee limits to operate $\leq 60^\circ$ flexion and the summation of quantified forces results in the required ATT recovery force.

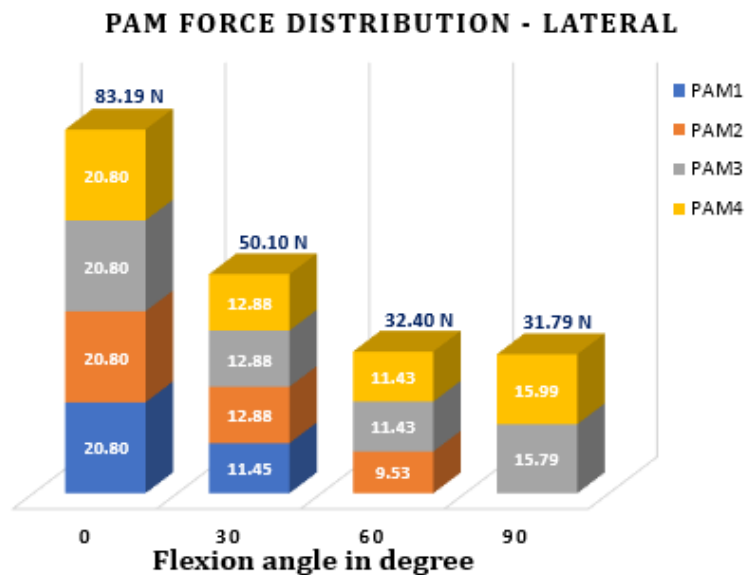


Figure 6.4: Distribution of total PAM forces in lateral side

6.3 Finite Element Simulation - Recovery Force

The recovery forces obtained by simulations from the Simscape model is expected to recover the ATT of an ACL ruptured knee to that of an intact knee. However, the model does not consider the complete model of the knee joint that involves several other structures such as soft tissues and ligaments into account. Thus, the effectiveness of these estimated forces needs to

be verified in a more realistic model as to compare with the analytical model presented in this study.

To verify this, finite element simulations are considered. Finite element model enables the simulation of patient-specific geometries involving hard and soft tissues thereby leading to a more realistic biomechanical behavior. In this research, the ACLD knee is subjected to the anterior loading force as well as the recovery force using the finite element model as in Figure 6.5 based on Naghibi et al. [2020].

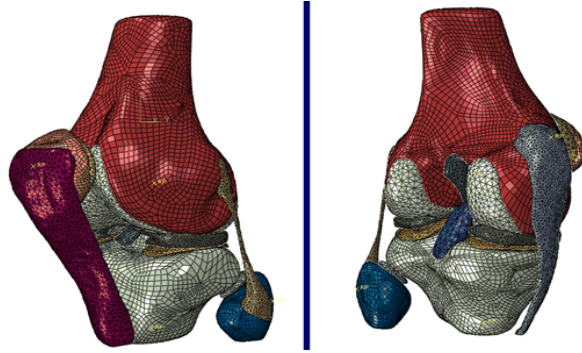


Figure 6.5: Finite element model of knee from Naghibi et al. [2020] to simulate anterior and recovery forces.

6.3.1 Recovered ATT

The recovery forces estimated in Section 6.1 are applied to the finite element model. The ATT and IE rotation observed before the application of recovery force corresponds to the ruptured knee. The results observed after application of recovery forces must ideally result in the ATT and IE of an ACL intact knee. Figure 6.6 presents the comparison of ATT in intact knee and the ATT observed in ruptured knee after the application of recovery force.

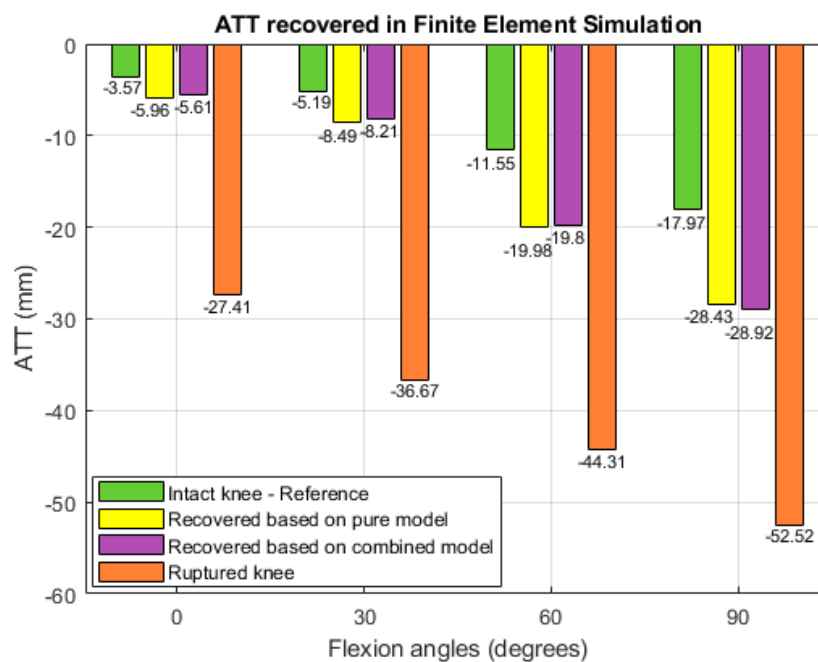


Figure 6.6: Evaluation of the effectiveness of the recovery forces calculated in this study in recovering ATT

Referring to Figure 6.6, the first bar from the left in every angle of flexion indicates the ATT in the ACL intact knee. The intact knee values act as reference values to compare the ATT values after the application of recovery force. The second and third bars represent the pure and combined ATT values respectively. The last bar shows the ATT in ruptured knee. From the obtained plot, it is evident that the ATT due to the laxity in an ACLD knee is considerably reduced after the application of recovery force.

The percentage recovery is compared by considering the ACL intact knee as the ideal case. The recovered ATT values from Figure 6.6 lie more towards the intact knee values indicating that the estimated recovery forces have significantly reduced the undesired ATT. The percentage of ATT that has been recovered from the ruptured knee condition is shown in Table 6.6. Highest recovery up to 91% is observed in flexion angles 0° and 30°, while the recovery has gradually reduced up to 68% in the flexion angles 60° and 90°.

Flexion angle (degrees)	Percentage recovery - ATT	
	Pure translation	Combined with IE
0	90	91
30	90	90
60	74	75
90	70	68

Table 6.6: Comparison of percentage recovery values

6.3.2 Recovered IE

ACL plays a crucial role in controlling the knee rotation (internal or external) at various flexion angles as mentioned in Section 2.2.2. To understand the direction of rotation, the values are represented by means of positive and negative axis. In this research, the values in positive axis represents the external rotation while the negative axis represents internal rotation. In the ACL intact condition, the rotations are mostly internal. With the loss of ACL, the internal rotations reduce and thereby more external rotations occur.

Figure 6.7 shows IE values in ruptured knee condition after the application of recovery force and compared with intact knee. The order of representation of the bars are similar to those represented in Figure 6.6. From the figure, the rotations are mostly internal for an intact knee but the ruptured knee is totally external. After the application of recovery force in pure and combined cases, the recovery is more towards the intact side meaning a higher recovery percentage.

Unlike the pure ATT, in ATT combined with IE, there is equal focus on both anterior translation and internal-external rotation. Thus, the recovery force in this case was focused to also recover the IE which is visible in Figure 6.7. The recovery force is directed to act on both medial and lateral sides of tibia to effectively recover the IE by reducing the undesired external rotation. The percentage recovery of the rotations is listed in Table 6.7.

From Table 6.7, the recovery in combined case is higher than pure translation case. This agrees with the previous statement that in combined translation, the recovery force is directed to also correct the undesired rotations in an ACLD knee. The recovery observed at 60° flexion in combined case shows that the applied recovery force has caused over-rotation leading to 110% recovery. This may be due to the presence of other structural constraints causing unsymmetrical rotation.

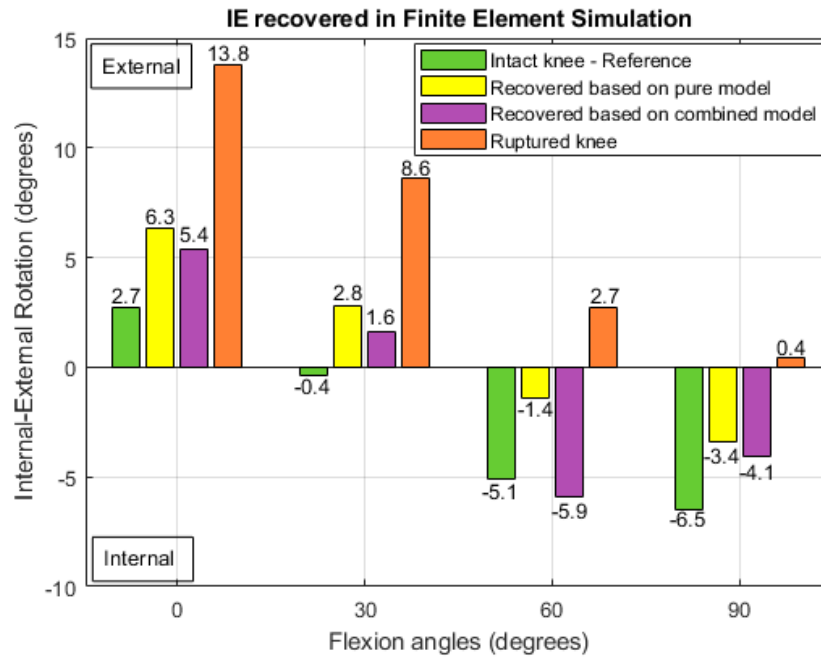


Figure 6.7: Evaluation of the effectiveness of the recovery forces calculated in this study in recovering IE

Flexion angle (degrees)	Percentage recovery - IE	
	Pure translation	Combined with IE
0	68	76
30	65	77
60	52	110*
90	55	65

Table 6.7: Comparison of percentage recovery values in IE

* Value above 100% indicates over-constrained condition.

7 Conclusions

This chapter provides the conclusion derived from the evaluations made in previous chapters. Next, the areas that could be improved with further study is discussed.

7.1 Conclusion

7.1.1 Research perspective

ACL plays a key role in maintaining the stability of the knee joint. With the loss of ACL, the impact on the stability of knee joint can be in one or more ways. Though ACL functions in the coordination with various other ligaments in the knee, the impact that follows the loss of ACL is significantly observed. This study focuses on evaluating the impact of ACL loss on anterior translation of tibia and internal-external rotation of tibia using an improved model of the soft robotic knee brace. To evaluate to performance of the design of the improved knee brace, the research questions are evaluated with the corresponding design goals to determine if the suggested improvement of design attempts to solve the underlying condition.

The first research question mentions the study of role of ACL in maintaining an optimal ATT by considering the morphological and neurological factors in ACL deficient knee. It is evident from the experiments that the position of ACL is such that it not only prevents the anterior motion of tibia but also in maintaining the undesired internal-external rotations in the joint that occurs as a result of different stiffness along the medial and lateral sides. Despite the fact that there are structural differences in medial and lateral condyles of the knee joint, the loss of ACL did add to the increased abnormalities in ATT and IE rotation.

Secondly, the contribution of muscle groups that act along with ACL in maintaining the stability of the knee joint is studied. It is implied through various previously conducted research that the hamstring muscle group plays a pivotal role by coordinating with ACL to maintain the stability of the joint. With the loss of ACL, the mechanism of hamstring muscles changes to produce forces more than the ones produced in intact ACL condition. The PAM forces estimated in the experiments are intended to share the additional load of the hamstring muscles thus contributing to cope for the loss of ACL.

The stiffness and damping factors of the knee joint affected by the loss of ACL are mentioned thirdly. The mathematical model helps to determine the stiffness of the joint using the applied force and ATT. However, the 2-link model also involves the damping factor. It is understood from the experiments that the stiffness and the damping factor are dependent on one another. The ATT is observed to be different for changed values in damping factor and stiffness. Through tests, it is revealed that the ATT values in intact knee are from higher values of damping while with ruptured ACL, the damping factor had to be reduced. Since the damping factor cannot be controlled in the joint, the stiffness parameter had to be varied to achieve normal ATT in this research. The divided anterior force on medial and lateral sides was chosen observing that division of forces equally and proportionately caused a significant difference in ATT in the simulated model.

Lastly, the effectiveness of the estimated forces is studied. The developed 2-link model recovered the ATT from ruptured to intact condition. This was however performed in the absence of more physiologically realistic conditions. To validate the correctness of the model, the finite element simulations are performed. The results from these simulations concluded that the recovery force was successful in overcoming the undesired ATT and IE up to an extent.

In the scope of this research, the recovery forces in the Simscape model and the finite element simulation are assumed to be transferred directly to the joint. However, the uncertainties

caused due to skin and soft-tissue deformation needs to be studied. This helps to expand the outcomes of this study to real-life applications.

7.1.2 Design perspective

From the design perspective, the knee brace prototype was improved in terms of redesign and modification of existing components. By retaining the concept design, the PAMs are modified to fit in the proposed new design layout. As the number of PAMs increases to act along all the discrete angles of flexion, the gaps between every PAM reduced. This posed a constraint on the design of clamps. The clamps are designed to hold the PAMs by not being bulky as in the previous design. The clamps can hold all the PAMs and withstand the axial forces exerted during its contraction. The screws in the front ensures proper gripping of the bi-layered cylinder while the shaft in the rear end ensures fixing the clamp to the support plates allowing rotation along its fixed axis. The stopper in the bottom of the clamps are designed to provide additional grip preventing the sliding of PAM downwards. Overall, the improved design is able to function in flexion angles 0° , 30° , 60° and 90° which is the design goal of this research.

7.2 Further improvements

The improved model of knee brace aimed at functioning in multiple angles of flexion to prevent ATT and IE rotation. However, the research could further be improved in the following aspects:

1. The functioning of the PAMs in multiple angles of flexion was achieved in a discrete fashion. To facilitate better analysis and convenience during gait cycle, it is recommended to improve the model to function
2. The application of anterior force is equally divided in ATT combined with IE. The approach could further be analysed by proportional division of forces.
3. Automating the calculation of recovery force reduces the time required to quantify the PAM forces.
4. The testing of the obtained results on an actual knee of healthy subjects is recommended. This helps to determine the effectiveness of the improved prototype.
5. Finally, the design could further be made compact with reduced number of PAMs but still be able to act in all the angles of flexion. An innovative joint mechanism could be studied and implemented to accompany this.

A Model Import: SolidWorks to Simscape

A.1 Initialization

- **Installations:**

1. Install Simscape Toolbox in MATLAB. The version used is R2020a.
2. Install Simscape Multibody Link in MATLAB.
3. Enable Simscape Multibody Link Plug-In in SolidWorks.

- **Model export from SolidWorks**

1. In the SolidWorks assembly, Tools > Simscape Multibody Link > Export > Simscape Multibody
2. Save as .xml file in the location where the assembly is saved. If the save is successful, MATLAB's command window appears.

- **Model import to MATLAB**

1. In MATLAB, open the directory where XML file is stored.
2. In command window, type `smimport('filename.xml')`. A Simulink window opens with the equivalent to the model imported from SolidWorks.
3. Save the .slx model before proceeding with further improvements.

A.2 Simscape model - Pure ATT (Figure 5.4)

This section explains the blocks in the SolidWorks equivalent model in Simscape in pure ATT case. To understand the blocks, Figure 5.2 and Figure 5.4 are compared.

Figure A.1 is the equivalent model, however with a few additional blocks after importing the model. The blocks within the blue dashed line are the *Default* blocks and within red dashed line are *Newly added* blocks.

A.2.1 Default blocks

Default blocks are those which are available directly once the model has been imported from Solidworks to Simscape. All the parts (P1, P2, P3) are recognized in the import task while one joint (J1) is imported. Apart from the parts and joints, there are other blocks in the model that are rather default and are used to define the relation between one-another blocks, denoted by **D(1–5)** series. For the model in Figure 5.2, **no parameters require changes in these blocks.** and are explained below:

1. **D1** - World frame that acts as the ground of all frame networks in the mechanical model.
2. **D2** - Mechanism configuration to specify uniform gravity - constant/time varying.
3. **D3** - Defines solver settings to use for simulation.
4. **D4** - 3-D rigid transformation between ground frame and fixed femur link.
5. **D5** - 3-D rigid transformation between ground frame and rotating tibia link. Rotation occurs between femur and tibia link if this block is removed.

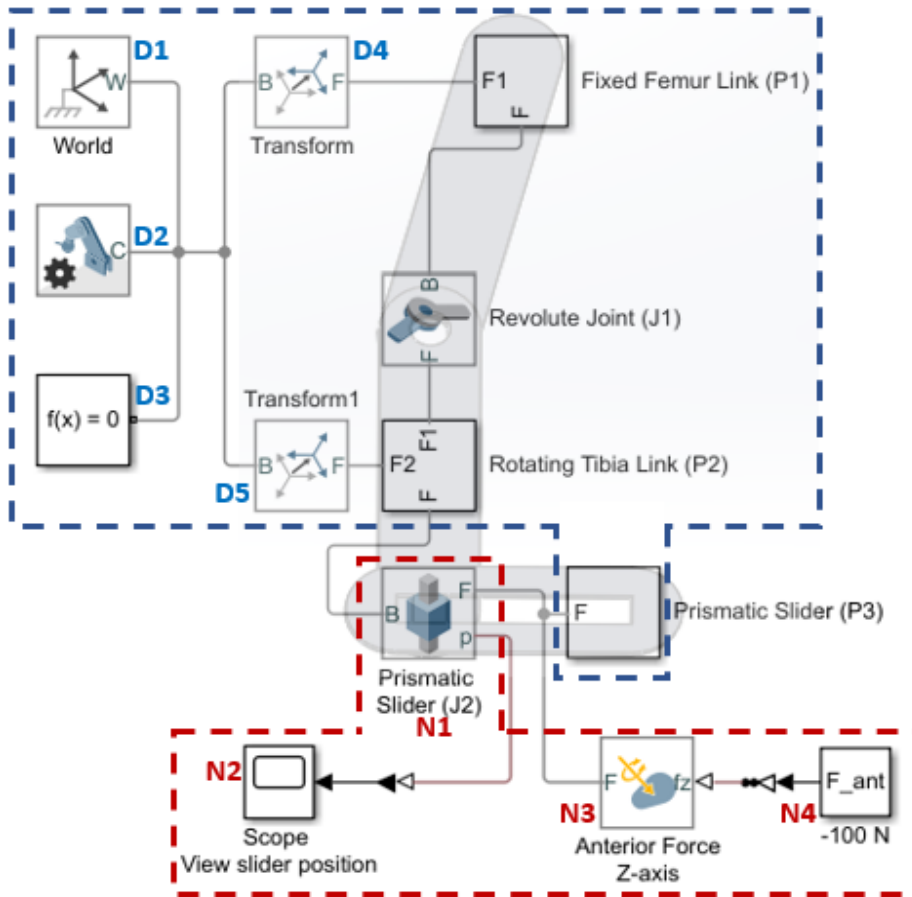


Figure A.1: Simscape model with categorized default (D) and newly added (N) blocks

A.2.2 Newly added blocks

Newly added blocks are those which are not available once the model has been imported from SolidWorks to Simscape. These blocks are externally added from the Simulink library to complete the mechanical model. All parts except prismatic joint (J2) are recognised from the SolidWorks model. Thus, prismatic joint (J2) is added externally since the connection between rotating tibia link (P2) and prismatic slider (P3) is initially rigid.

In Figure A.1, **N(1 – 4)** series are the newly added blocks. The input to these blocks and descriptions are explained below:

1. **N1** - *Prismatic slider* joint is not recognized during the import and should be added externally. In properties, the internal mechanics contains the stiffness and damping coefficient of the model. The values are specified as discussed in Section 5.2. The units which are predefined in metres (m) is changed to millimetres (mm). The properties also contains limits through which the maximum and minimum extent of translation is specified. The upper and lower bound is set as per the length of the prismatic slider. The sensing is set to measure position (p)
2. **N2** - The position (p) of prismatic slider is measured in *scope*. The signal from J2 is fed to *scope* through PS-Simulink converter. The output signal unit in the converter block is specified in millimetres.

3. **N3** - *External force or torque* block is added to apply the anterior force on the slider joint. In properties, 'Force(Z)' must be checked to apply the anterior force in z-direction in this model.
4. **N4** - *Constant* block specifies the quantity of force that is applied to the prismatic joint through N3 block.

A.3 Simscape model - ATT combined with IE (Figure 5.7)

A.3.1 Medial-Lateral representative translations

Figure A.2 shows the Simscape equivalent model of Figure 5.7. Similar to the approach used in Section A.2, the figure has been categorized into default and newly added blocks. The difference would be that the earlier approach is the pure translation model with a single 2-link design while the latter has two 2-link designs placed parallel to one another to show medial and lateral representative translations. There are no new constraints in the default (D) or the newly added (N) blocks apart the ones defined in Section A.2.1 and Section A.2.2.

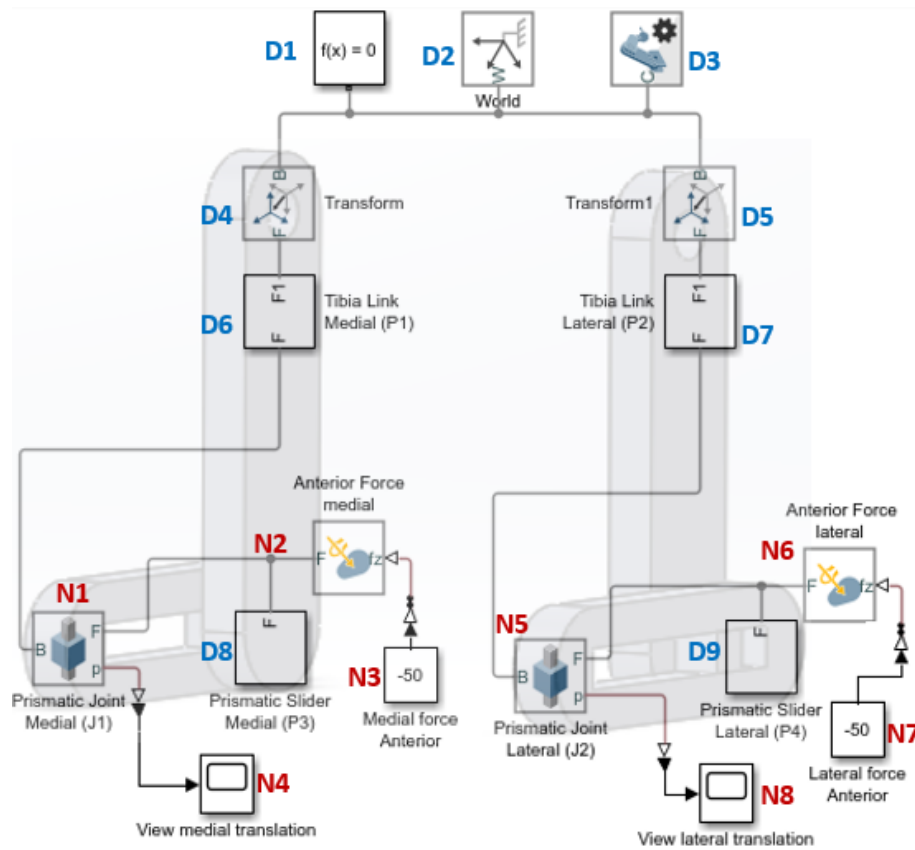


Figure A.2: Simscape model with categorized default (D) and newly added (N) blocks

A.3.2 Medial-Lateral representative translations with recovery force

In ATT combined with IE, there are two anterior and recovery forces. One each acting along medial and lateral sides. The medial and lateral anterior force are chosen to be -50N each. The values of medial and lateral recover forces can vary based on flexion angles from *Sum* values in Table 6.2 and Table 6.4 respectively.

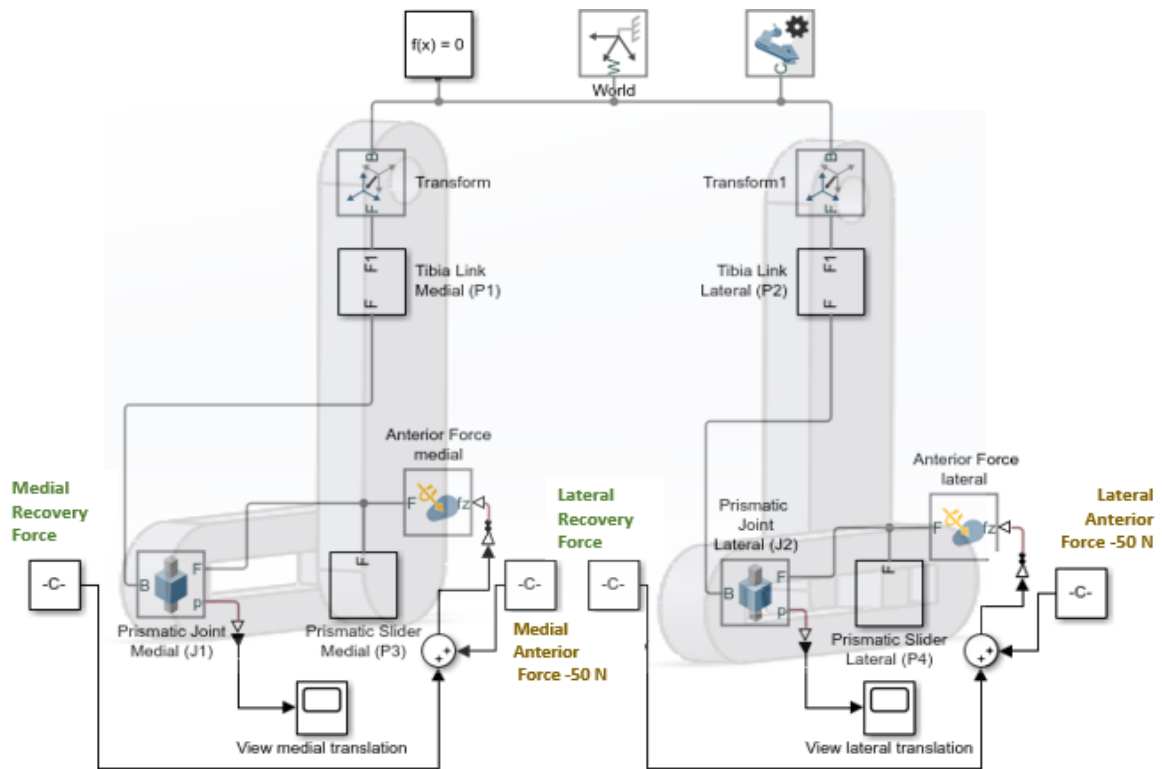


Figure A.3: Simscape model with added medial and lateral recovery force blocks

Bibliography

- S Aalbersberg, I Kingma, and J van Dieën. Hamstrings co-activation in ACL-deficient subjects during isometric whole-leg extensions. *Knee Surgery, Sports Traumatology, Arthroscopy*, 17(8):946–955, 2009. ISSN 09422056. doi: 10.1007/s00167-009-0802-4.
- R L Begalle, L J DiStefano, T Blackburn, and D A Padua. Quadriceps and hamstrings coactivation during common therapeutic exercises. *Journal of Athletic Training*, 47(4):396–405, 2012. ISSN 10626050. doi: 10.4085/1062-6050-47.4.01.
- B D Beynnon and B C Fleming. Anterior cruciate ligament strain in-vivo: a review of previous work. *Journal of biomechanics*, 31(6):519–25, 1998. ISSN 0021-9290. doi: 10.1016/S0021-9290(98)00044-x.
- B D Beynnon, C M Wertheimer, J Johnson, B C Fleming, C E Nichols, J G Howe, McClure Musculoskeletal, Everett Bone, Joint Physicians, Pacific Avenue, and Medical Building. The Effect of Functional Knee-Braces on Strain on the Anterior Cruciate Ligament in Vivo. *J Bone Joint Surg Am*, 74(9):1298–1312, 1992.
- O C Brantigan and A F Voshell. The mechanics of the ligaments and menisci of the knee joint. *Journal of Bone & Joint Surgery*, 23(1):44–66, 1941.
- A L Bryant, M W Creaby, R U Newton, and J R Steele. Dynamic Restraint Capacity of the Hamstring Muscles Has Important Functional Implications After Anterior Cruciate Ligament Injury and Anterior Cruciate Ligament Reconstruction. *Archives of Physical Medicine and Rehabilitation*, 89(12):2324–2331, 2008. ISSN 00039993. doi: 10.1016/j.apmr.2008.04.027.
- M Buckthorpe, G La Rosa, and F D Villa. Restoring Knee Extensor Strength After Anterior Cruciate Ligament Reconstruction: a Clinical Commentary. *International Journal of Sports Physical Therapy*, 14(1):159–172, 2019. ISSN 2159-2896. doi: 10.26603/ijsp20190159.
- D Butler, F Noyes, and E S Grood. Ligamentous restraints to anterior-posterior drawer in the human knee: A biomechanical study. *Classic Papers in Orthopaedics*, 62(May 2014):141–143, 1980. ISSN 0021-9355. doi: 10.1007/978-1-4471-5451-8{_}34.
- F Daerden and D Lefeber. Pneumatic artificial muscles: Actuators for robotics and automation. *European Journal of Mechanical and Environmental Engineering*, 47(1):11–21, 2002. ISSN 00353612.
- J Dargel, M Gotter, K Mader, D Pennig, J Koebke, and R Schmidt-Wiethoff. Biomechanics of the anterior cruciate ligament and implications for surgical reconstruction. *Strategies in Trauma and Limb Reconstruction*, 2(1):1–12, 2007. ISSN 18288936. doi: 10.1007/s11751-007-0016-6.
- M S Dhillon, K Bali, and S Prabhakar. Proprioception in anterior cruciate ligament deficient knees and its relevance in anterior cruciate ligament reconstruction. *Indian Journal of Orthopaedics*, 45(4):294–300, 2011. ISSN 00195413. doi: 10.4103/0019-5413.80320.
- Doc Ortho. Knee Braces & Supports, 2020. URL <https://www.docortho.com/collections/knee-braces-supports>.
- D J Dutto and G A Smith. Changes in spring-mass characteristics during treadmill running to exhaustion. *Med Sci Sports Exerc*, 34(8):1324–31, 2002. doi: 10.1097/00005768-200208000-00014.
- Y Feng, T Y Tsai, J S Li, S Wang, H Hu, C Zhang, H E Rubash, and G Li. Motion of the femoral condyles in flexion and extension during a continuous lunge. *Journal of Orthopaedic Research*, 33(4):591–597, 2015. ISSN 1554527X. doi: 10.1002/jor.22826.
- S Hirokawa, M Solomonow, Z Luo, Y Lu, and R D’Ambrosia. Muscular co-contraction and control of knee stability. *Journal of Electromyography and Kinesiology*, 1(3):199–208, 1991. ISSN 10506411. doi: 10.1016/1050-6411(91)90035-4.

- H Johansson, P Sjölander, and P Sojka. Receptors in the knee joint ligaments and their role in the biomechanics of the joint. *Crit Rev Biomed Eng.*, 18(5):341–68, 1991.
- C D S Jones and P N Grimshaw. The Biomechanics of the Anterior Cruciate Ligament and Its Reconstruction. In *Theoretical Biomechanics*, pages 361–384. InTech, 2011. doi: 10.5772/19939.
- H.M. Khambati. A soft robotic knee brace for improving stability in anterior cruciate ligament deficient patients, Master Thesis, University of Twente, 2019.
- P Kousa, E C Argentieri, and B D Beynnon. *Anterior Cruciate Ligament Strain Behavior During Rehabilitation Exercises*. Elsevier, 2 edition, 2018. ISBN 9780323497398. doi: 10.1016/B978-0-323-38962-4.00108-9.
- R Y Lam, G Y Ng, and E P Chien. Does wearing a functional knee brace affect hamstring reflex time in subjects with anterior cruciate ligament deficiency during muscle fatigue? *Archives of Physical Medicine and Rehabilitation*, 83(7):1009–1012, 2002. ISSN 00039993. doi: 10.1053/apmr.2002.33231.
- J M Lipke, C J Kanecki, and C L Nelson. The role of incompetence of the anterior cruciate and lateral ligaments in anterolateral and anteromedial instability. A biomechanical study of cadaver knees. *The Journal of Bone and Joint Surgery*, 63(6):954–960, 1981.
- W Liu and M E Maitland. The effect of hamstring muscle compensation for anterior laxity in the ACL-deficient knee during gait. *Journal of Biomechanics*, 33(7):871–879, 2000. ISSN 00219290. doi: 10.1016/S0021-9290(00)00047-6.
- A D Lynch, D S Logerstedt, M J Axe, and L Snyder-Mackler. Quadriceps Activation Failure After Anterior Cruciate Ligament Rupture Is Not Mediated by Knee Joint Effusion. *Orthop Sports Phys Ther.*, 42(6):1–19, 2012. ISSN 15378276. doi: 10.2519/jospt.2012.3793.
- B A MacWilliams, D R Wilson, J D Desjardins, J Romero, and E Y S Chao. Hamstrings co-contraction reduces internal rotation, anterior translation, and anterior cruciate ligament load in weight-bearing flexion. *Journal of Orthopaedic Research*, 17(6):817–822, 1999. ISSN 07360266. doi: 10.1002/jor.1100170605.
- M Marieswaran, I Jain, B Garg, V Sharma, and D Kalyanasundaram. A review on biomechanics of anterior cruciate ligament and materials for reconstruction. *Applied Bionics and Biomechanics*, 2018:1–14, 2018. ISSN 17542103. doi: 10.1155/2018/4657824.
- Mathworks. Simscape Multibody, 2020. URL <https://nl.mathworks.com/products/simmechanics.html>.
- S Miller. The Best Knee Braces For Torn ACL & Meniscus, 2020. URL <https://www.mostcraft.com/best-knee-brace-for-torn-acl/>.
- M Mori, K Suzumori, M Takahashi, and T Hosoya. Very high force hydraulic McKibben artificial muscle with a p-phenylene-2,6-benzobisoxazole cord sleeve. *Advanced Robotics*, 24(1-2): 233–254, 2010. ISSN 01691864. doi: 10.1163/016918609X12586209967366.
- H Naghibi, D Janssen, T Van Tienen, S Van de Groes, T Van de Boogaard, and N Verdonshot. A novel approach for optimal graft positioning and tensioning in anterior cruciate ligament reconstructive surgery based on the finite element modeling technique. *The Knee*, 27(2):384–396, 2020. ISSN 18735800. doi: 10.1016/j.knee.2020.01.010.
- NHS Foundation. Anterior cruciate ligament deficient (ACLD) knee, 2020. URL <https://www.guysandstthomas.nhs.uk/resources/patient-information/therapies/physiotherapy/acld-knee.pdf>.
- F R Noyes and S D Barber-Westin. *Noyes' Knee Disorders: Surgery, Rehabilitation, Clinical Outcomes*. Second edition, 2017. ISBN 9780323329033. doi: 10.1016/C2013-0-18673-4.
- OrthoInfo. Anterior Cruciate Ligament (ACL) Injuries, 2014. URL <https://orthoinfo.aaos.org/en/diseases--conditions/>

- [anterior-cruciate-ligament-acl-injuries/](#).
- A Papadonikolakis, L Cooper, N Stergiou, A D Georgoulis, and P N Soucacos. Compensatory mechanisms in anterior cruciate ligament deficiency. *Knee Surgery, Sports Traumatology, Arthroscopy*, 11(4):235–243, 2003. ISSN 09422056. doi: 10.1007/s00167-003-0367-6.
- M V Paterno. Non-operative Care of the Patient with an ACL-Deficient Knee. *Current Reviews in Musculoskeletal Medicine*, 10(3):322–327, 2017. ISSN 19359748. doi: 10.1007/s12178-017-9431-6.
- S C Petterson, P Barrance, T Buchanan, S Binder-Macleod, and L Snyder-Mackler. Mechanisms underlying quadriceps weakness in knee osteoarthritis. *Medicine and Science in Sports and Exercise*, 40(3):422–427, 2008. ISSN 01959131. doi: 10.1249/MSS.0b013e31815ef285.
- H H Rachmat, D Janssen, G J Verkerke, R L Diercks, and N Verdonschot. In-situ mechanical behavior and slackness of the anterior cruciate ligament at multiple knee flexion angles. *Medical Engineering and Physics*, 38(3):209–215, 2016. ISSN 18734030. doi: 10.1016/j.medengphy.2015.11.011.
- B T Raines, E Naclerio, and S L Sherman. Management of Anterior Cruciate Ligament Injury?: What's In and What's Out? *Indian Journal of Orthopaedics*, 51(5):563–575, 2017. doi: 10.4103/ortho.IJOrtho{_}245{_}17.
- E Roche. Pneumatic Artificial Muscles, 2020. URL <https://softroboticstoolkit.com/book/pneumatic-artificial-muscles>.
- D K Schneider, A Gokeler, B Otten, K R Ford, T E Hewett, J Divine, A J Colosimo, Robert S Heidt, and G D Myer. A Novel Mass-Spring-Damper Model Analysis to Identify Landing Deficits in Athletes Returning to Sport after ACL Reconstruction. *Journal of Strength and Conditioning Research*, 31(9):2590–2598, 2017. ISSN 1064-8011. doi: 10.1519/JSC.0000000000001569.A.
- K B Shelburne, M R Torry, and M G Pandy. Effect of muscle compensation on knee instability during ACL-deficient gait. *Medicine and Science in Sports and Exercise*, 37(4):642–648, 2005. ISSN 01959131. doi: 10.1249/01.MSS.0000158187.79100.48.
- P N Smith, K M Refshauge, and J M Scarvell. Development of the Concepts of Knee Kinematics. *Archives of Physical Medicine and Rehabilitation*, 84(12):1895–1902, 2003. ISSN 00039993. doi: 10.1016/S0003-9993(03)00281-8.
- Memorial Hermann IRONMAN Sports Medicine Institute. Anterior Cruciate Ligament (ACL) Surgery, 2020. URL <http://ironman.memorialhermann.org/sports-injuries/knee-injuries/acl-surgery/>.
- Stratasys. Agilus30, 2018. URL <https://www.stratasys.com/materials/search/agilus30>.
- G N Williams, L Snyder-Mackler, P J Barrance, and T S Buchanan. Quadriceps femoris muscle morphology and function after ACL injury: A differential response in copers versus non-copers. *Journal of Biomechanics*, 38(4):685–693, 2005. ISSN 00219290. doi: 10.1016/j.jbiomech.2004.04.004.
- C Wilson. Foot Cramps, 2019. URL <https://www.foot-pain-explored.com/foot-cramps.html>.
- x10therapy. The Fundamental Importance of Knee Range of Motion, 2020. URL <https://x10therapy.com/knee-range-of-motion/>.
- S A Xergia, F Zampeli, E Tsepis, N K Paschos, E Pappas, and A Georgoulis. *Nonoperative Management of Anterior Cruciate Ligament Deficient Patients*. Elsevier, 3 edition, 2018. ISBN 9780323497398. doi: 10.1016/B978-0-323-38962-4.00011-4.